21GRD02 BIOSPHERE

D7: Report on the assessment of the effect on healthy human cells of exposure to environmental level single and combined SCR and UV radiation fields under experimental conditions based on the measurement of induced stress gene expression changes using system biology approaches

Organisation name of the lead participant for the deliverable: **IVB**

Due date of the deliverable: **Nov 2024** (M26)

Actual submission date of the deliverable: 30 September 2025

Funded by the European Union. Views and opinions expressed are however those of the author(s) only and do not necessarily reflect those of the European Union or EURAMET. Neither the European Union nor the granting authority can be held responsible for them.

The project has received funding from the European Partnership on Metrology, co-financed from the European Union's Horizon Europe Research and Innovation Programme and by the Participating States.

Glossary

ASTM, American Society for Testing and Materials;

CRL 9855, human monocyte cell line;

CTRL, laboratory control (cells kept in the biology laboratory during the experiment);

DAPI, 4′6-diamidino-2-phenylindole; DDR, DNA damage response;

DMEM, Dulbecco's modified Eagle's medium;

DNA, deoxyribonucleic acid;

DPBS, Dulbecco’s phosphate buffered saline; DSBs,

DNA double-strand breaks;

EDTA, ethylenediaminetetraacetic acid;

FBS, fetal bovine serum;

FC, fold change;

GO, Gene Ontology;

H2AX, H2A histone family member X;

HaCaT, human keratinocyte cell line;

Hs27, human skin fibroblast cell line;

IF, immunofluorescence;

IgG, immunoglobulin G;

IMDM, Iscove's Modified Dulbecco's Medium;

IrrCTRL, control cells kept in the irradiation room during the experiment;

LDH, lactate dehydrogenase;

MED, minimal erythema dose;

MTS, 3-(4,5-dimethylthiazol-2-yl)-5-(3-carboxymethoxyphenyl)-2-(4-sulfophenyl)-2H-tetrazolium;

NER, nucleotide excision repair;

OD, optical density;

PBS, phosphate buffered saline;

RT, room temperature;

SCR, secondary cosmic rays;

SD, standard deviation;

SEM, standard error of the mean;

qRT-PCR, quantitative real-time polymerase chain reaction;

UV, ultraviolet radiation;

UVA, ultraviolet A radiation;

UVB, ultraviolet B radiation.

Contents

1 Summary

The assessment of the long-term effects of normal human tissues/cells after exposure to complex radiation fields, resulting from large solar particle events in conjunction with ground-level enrichment due to ozone depletion, is a challenge for radiobiological research that needs to be addressed. This is important not only to understand cells' radiosensitivity, but also to make informed decisions about the global challenges facing our society nowadays.

The goal of the study was to investigate the mutual effects of combined radiation fields (cosmic rays and solar UVB radiation) at the level of stress genes expression changes in human normal (non-cancerous) skin and blood cells that were experimentally exposed to energetic protons and UVB radiation in well-controlled irradiation settings, and to place gene expression changes in the context of cellular viability decrease, and DNA damage.Human Hs27 fibroblasts, HaCaT keratinocytes, and CRL 9855 monocytes were exposed to energetic protons (0.5 Gy) and UVB (50 J/m2) as single or combined radiation (protons first, and then, within approximately 20 min, to UVB), in well-controlled irradiation conditions. The expression changes of 84 stress genes in irradiated cells compared to unexposed control cells were assessed by RT-PCR using a pathway-focused array and five housekeeping genes as references. Gene expression changes were analyzed in relation to cellular viability, assessed using the MTS reduction and lactate dehydrogenase release assays, and in relation to DNA damage, evaluated by γH2AX immunofluorescence. The network of over-expressed stress genes was built using the STRING software.The synergistic action of protons and UVB was highlighted at the level of DNA damage in Hs27 fibroblasts and HaCaT keratinocytes, as compared with single radiation. This was translated into a slight decrease in the number of metabolically active cells. The viability of keratinocytes and monocytes was dictated by the UVB effects, while a synergistic action of protons and UVB was demonstrated in fibroblasts. DNA damage peaked at 3-6 hours post-irradiation and decreased at 24 h, when residual DNA damage was evident. The gene expression study indicated that exposed cells remained under stress even at 48 h, with some repair mechanisms related to DNA damage, oxidative stress, hypoxic stress, endoplasmic reticulum stress, and inflammation still active. Meanwhile, other mechanisms were down-regulated as an attempt to resolve the stress response. The gene expression pattern in cells co-exposed to protons and UVB reproduced the pattern induced by single radiation; however, additional genes were found to be upregulated in co-exposed fibroblasts, and to a lesser extent, in keratinocytes. The stress response of monocytes at the gene expression level was dictated by UVB. Inflammation-related genes were upregulated in both immune and non-immune cells investigated.A prolonged stress was evidenced in human normal keratinocytes, fibroblasts, and monocytes exposed in vitro to combined proton and UVB radiation as a mimic of increased human exposure to combined radiation fields reaching the Earth due to the progressive depletion of the stratospheric ozone layer. Co-exposure of cells inflicted more profound and persistent DNA damage than either radiation alone. Gene targets, common or specific to each cell line, were identified for further shaping a therapeutic strategy aimed at alleviating the harmful effects of combined radiation exposure.

Introduction

During geomagnetic storms and solar particle events, high-energy particles can lead to the production of chemically active nitrogen and hydrogen oxides that are known to be associated with the catalytic breakdown of ozone[1]. As ozone protects the Earth from harmful ultraviolet (UV) rays from the Sun, its depletion would lead to an increase in biologically active UV radiation flux, with a significant impact on the terrestrial environment and human health.

Cosmic rays and the Earth's natural radioactivity, along with the UV radiation, are critical sources of atmospheric ionisation that greatly affects human health either through direct exposure to complex radiation fields, or through the indirect impact of the climate system change in general.

Ionisation of the biosphere by cosmic radiation (solar particle events and galactic cosmic rays) is known to correlate significantly with disease prevalence in humans, having the potential to affect, depending on the

[1] Mironova IA, et al., Energetic Particle Influence on the Earth's Atmosphere, Space Sci Rev 2015;194:1–96.

context, all the organs and systems of the human body by exerting targeted and non-targeted actions[2]. Chronic exposure to low-dose radiation became lately a concern in the context of solar events and the thinning of the ozone layer, being associated with adverse health outcomes, including increased risk to develop cancer, cardiovascular diseases, neurological disorders, immune dysfunctions, eye disorders, and heritable genetic effects. Alteration of the body's homeostasis and the increased risk to develop chronic diseases and cancer were shown to occur even at low doses of radiation[3,4].

These adverse effects of cosmic radiation exposure are complemented by the harmful effects caused by UV radiation, such as an increased incidence of skin cancer, especially in light-skinned populations, by about 2% for every 1% reduction in the depth of the ozone layer. According to data from the Global Burden of Disease Study, the incidence of skin cancers in 2019 was estimated at 4 million cases of basal cell carcinoma, 2.4 million cases of squamous cell carcinoma, and 0.4 million cases of melanoma[5] [6]. Moreover, prolonged exposure to UV radiation has been shown to contribute to the development of cataracts and other eye diseases that are responsible for a large proportion of visual impairment world-wide[7]. The ozone layer is essential for protecting life on Earth against the harmful UVB radiation, and its depletion poses serious risks to human health, ecosystems, and materials. UVB radiation (280–315 nm), a component of sunlight, has been identified as a primary factor causing various skin conditions such as erythema and oedema[8]. The minimal erythema dose (MED) for UVB radiationis between 20 mJ/cm^2 and 60 mJ/cm^2. In contrast, the MED for UVA radiation is approximately a thousand times higher[9]. To illustrate the effect of atmosphere in the UVB part of the solar spectrum, Figure 1 shows the reference AM 1.5 spectra defined by the American Society for Testing and Materials (ASTM), as well as the difference between the solar spectrum, and the direct spectrum that considers only the direct component of sunlight, ignoring any diffuse radiation. The total UVB flux density blocked by the atmosphere is about 1.7 mW/cm^2. Stratospheric ozone depletion causes some of this energy to leak to the terrestrial surface, and this is inciting an increased risk of non-melanoma and melanoma skin cancers, the development of cataracts, and changes in the immune responses. Additionally, photoaging is primarily caused by UVB radiation, although UVA radiation can also contribute to this effect[10].

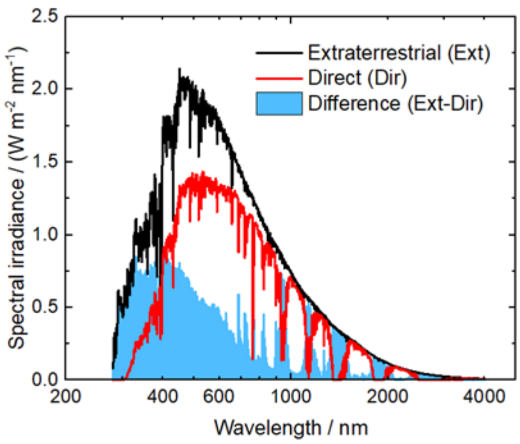

Figure 1. The reference AM 1.5 spectra defined by the American Society for Testing and Materials (ASTM)

---

[2]Talapko J, Talapko D, Katalinić D, Kotris I, Erić I, Belić D, Vasilj Mihaljević M, Vasilj A, Erić S, Flam J, Bekić S, Matić S, Škrlec I. Health Effects of Ionizing Radiation on the Human Body. Medicina (Kaunas). 2024;60(4):653. doi: 10.3390/medicina60040653.

[3] National Academies of Sciences, Engineering, and Medicine; Division on Earth and Life Studies; Nuclear and Radiation Studies Board; Committee on Developing a Long-Term Strategy for Low-Dose Radiation Research in the United States. Leveraging Advances in Modern Science to Revitalize Low-Dose Radiation Research in the United States. Washington (DC): National Academies Press (US); 2022 Oct 20.

[4] Shin E, Lee S, Kang H, Kim J, Kim K, Youn H, Jin YW, Seo S, Youn B. Organ-Specific Effects of Low Dose Radiation Exposure: A Comprehensive Review. Front Genet. 2020;11:566244. doi: 10.3389/fgene.2020.566244.

[5] Leiter U, Keim U, Garbe C. Epidemiology of Skin Cancer: Update 2019. Adv Exp Med Biol. 2020;1268:123-139. doi: 10.1007/978-3-030-46227-7_6.

[6] Zhang W, Zeng W, Jiang A, He Z, Shen X, Dong X, Feng J, Lu H. Global, regional and national incidence, mortality and disability-adjusted life-years of skin cancers and trend analysis from 1990 to 2019: An analysis of the Global Burden of Disease Study 2019. Cancer Med. 2021;10(14):4905-4922. doi: 10.1002/cam4.4046.

[7] Roberts JE. Ultraviolet radiation as a risk factor for cataract and macular degeneration. Eye Contact Lens. 2011;37(4):246-9. doi: 10.1097/ICL.0b013e31821cbcc9.

[8] de Gruijl, F.R.; Longstreth, J.; Norval, M.; Cullen, A.P.; Slaper, H.; Kripke, M.L.; Takizawa, Y.; van der Leun, J.C. Health effects from stratospheric ozone depletion and interactions with climate change. Photochem Photobiol Sci 2003; 2:16-28, doi:10.1039/b211156j.

[9] Sutherland, B.M.; Hacham, H.; Sutherland, J.C.; Gange, R.W. Pyrimidine dimer formation by UVA radiation: Implications for photoreactivation. 1991.

[10] Gromkowska-Kępka, K.J.; Puścion-Jakubik, A.; Markiewicz-Żukowska, R.; Socha, K. The impact of ultraviolet radiation on skin photoaging - review of in vitro studies. J Cosmet Dermatol 2021;20, 3427-3431, doi:10.1111/jocd.14033.

Aim of the biological study

The assessment of the long-term effects of normal human tissues/cells after exposure to combined exposures to complex radiation fields that could result from large solar particle events in conjunction with ground-level enrichment due to ozone depletion, as well as the investigation of the underlying cellular mechanisms that are potentially responsible for the disturbed behaviour of normal cells/tissues under complex irradiation is a challenge for radiobiological research that need to be addressed. This is important not only to understand the radiosensitivity of cells, but also to make informed decisions about the global challenges facing our society.

To answer this challenge, the goal of the study was to investigate the mutual effects of combined radiation fields (cosmic rays and solar UVB radiation) at the level of stress genes expression in human normal (non-cancerous) skin and blood cells that were experimentally exposed to energetic protons and UVB radiation in well-controlled irradiation settings, and to place gene expression changes in the context of cellular viability decrease, and DNA damage.

2 Materials and methods

Human non-cancerous cell lines

Human HaCaT keratinocytes were purchased for CLS Cell Line Services GmbH (Eppelheim, Germany), while human Hs27 skin fibroblasts (CRL-1634) and human peripheral blood monocytes (CRL 9855, US Pat. No. 5.447.861) were obtained from ATCC (Manassas, VA, USA). Cells were cultivated according to the recommendations of the depositor. Thus, the adherent cell lines HaCaT and Hs27 were cultivated in Dulbecco's modified Eagle's medium (DMEM, 12491015, Life Technologies, Burlington, Canada) supplemented with 10% fetal bovine serum (FBS, A3160401, Life Technologies, Burlington, Canada), with passage 2-3 times per week using Trypsin/EDTA 0.05%/0.02% in phosphate buffered saline (PBS), w/o Ca^{2+} and Mg^{2+} (P10-023100, PAN Biotech GmbH, Aidenbach, Germany). The non-adherent CRL 9855 monocytes were grown in Iscove's Modified Dulbecco's Medium (12440053, IMDM, Life Technologies, Burlington, Canada) containing 10% FBS, 1% HT supplement (10 mM sodium hypoxanthine and 1.6 mM thymidine) (11-067-030, Gibco, Life Technologies, Burlington, Canada), 1% 2-mercaptoethanol (21985023, Gibco, Life Technologies, Burlington, Canada), and 1% antibiotic-antimycotic solution (100X) (A5955, Sigma-Aldrich, Saint Louis, USA). Cells were passaged 3 times per week by addition of fresh complete culture medium for keeping cellular density between 0.35 – 1.30 x 10^6 cells/mL.

Preparation of cells for exposure to protons and UVB

Cells at passages 8-16, with a viability > 90% were used in experiments. Briefly, adherent HaCaT and Hs27 cells were detached with Trypsin/EDTA 0.05%/0.02% (P10-023100, PAN Biotech GmbH, Aidenbach, Germany). All the cell suspensions (HaCaT, Hs27 and CRL 9855) were centrifuged and suspended in RPMI 1640 culture medium w/o phenol red (11835030, Gibco, Life Technologies, Burlington, Canada), supplemented with 10% FBS. Cells were counted using a Burker-Turk counting chamber, and viability was assessed by the trypan blue exclusion test. Finally, cells were suspended in RPMI 1640 culture medium without phenol red at a cell density of 0.7 x 10^7 cells/mL for HaCaT or Hs27 cells, and 10^7 cells/mL for CRL 9855 monocytes. Finally, 100 µL of cell suspension were placed in a well of a low adhesion 48 well plate (677102, Cellstar, Greiner Bio One, Kremsmünster, Austria) or in a special dish on a 25 µm thick biofoil dish described in Figure 2 for proton exposure top-to-bottom or bottom-to-top, respectively. Separate samples were prepared for UVB or proton exposure as well as samples for successive co-exposure to protons and UVB. Various appropriate non-irradiated controls, containing cells that were handled like the irradiated ones, were used. The irradiation control was kept in the irradiation room during the irradiation experiment (IrrCTRL), outside the proton beam, while the lab control (CTRL) was kept in the biology laboratory, outside the irradiation room. Co-exposed samples were first irradiated with protons, and approximately. 20 min thereafter to UVB. Cells exposed to protons in low adhesion 48-well plates were directly transferred to UVB exposure, whilst cells, placed in the above-described dishes for proton exposure, were transferred first to low adhesion 48-well plates, and were exposed to UVB thereafter.

Irradiation of cells

Proton irradiation

Proton irradiations with nominal 10 MeV were carried out at the PTB ion accelerator facility[11]. A compact cyclotron was used to produce the proton beam with an initial energy of 14.85 MeV ± 0,08 MeV. To deliver a homogenous proton fluence over the entire cell layer, a part of the primary proton beam was scattered by a 28 µm thick Tantalum foil (5 µm thick gold foil) in the center of a scattering chamber. The cells were positioned at an angle of 90°, at 183 mm at the bottom in a 48-well plate, and at 185 mm at the top of the chamber in the special dish (Figure 2).

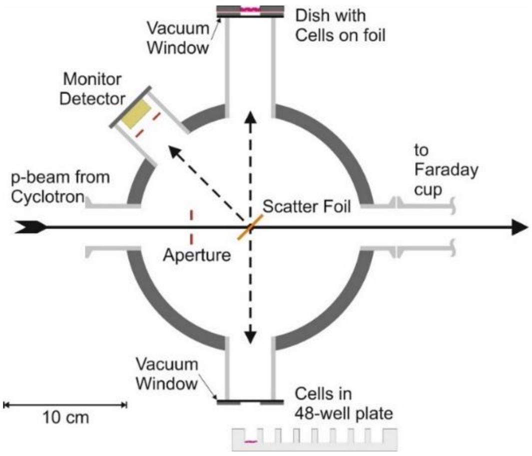

Figure 2. Schematic overview of the proton irradiation setup.

Protons underwent energy losses while passing the scattering foil, the vacuum seal (5 µm and 7 µm Molybdenum foil), an air gap of 31 mm, and 1 mm of medium at the bottom, or the 25 µm biofoil at the top. A 500 µm Aluminum absorber was added on top to provide the same proton energy at both positions after the different energy losses. The final proton energy of the protons at the cell layers was calculated with the SRIM-2013 software[12] to 9.7 MeV ± 0,4 MeV, with a calculated LET of 4.8 ± 0.2 keV/µm at the bottom, and 9.6 MeV ± 1 MeV, with a calculated LET of 4.9 ± 0.4 keV/µm at the top position (this difference results from the different path of the ions through the scatter foil and a different effective thickness and energy loss). Calculations were based on the nominal thickness of the foils, the measured thickness of the Aluminum absorber, and the volume of the medium in the well. The dose applied to cells was calculated from the LET-value and the proton fluence, which was determined from control measurements of scattered protons at both positions. It was simultaneously monitored with a particle detector at 135 degrees. The integrated proton beam charge, collected at the Faraday cup, provided a further monitor. Typical beam currents were 0.3 µA, and the typical dose rate was around 30 mGy/ min (0.7 µA and 15 mGy/min with the thinner foil). The uncertainty in the dose values is 7.5% for irradiations at the bottom position and 10.3% at the top.

The interaction of the primary proton beam with the material of slits, the aperture, and in the Faraday cup produced a neutron and gamma background of about 14 mGy per Gy of proton dose delivered to cells, as measured with a tissue-equivalent ionization chamber (Exradin, Model T2) close to the bottom position of cells.

Exposure of cells to a low-radiation background

To assess the impact of the natural radiation background, human normal cells (HaCaT keratinocytes) were cultivated either in the biology laboratory of IVB or in the Laboratory of IFIN “Horia Hulubei” in the Unirea salt mine situated in Slanic-Prahova, Romania, 208 m underground, with a low radiation background:

- Absorbed dose rate in the mine laboratory: (1.17 ± 0.14) nGy/h vs (87.8 ± 27.4) nGy/h at the surface;
- Gamma spectrum reduced by ~100× (40 keV–3 MeV) in the mine laboratory:
    - Total gamma count rate in the laboratory: 2.19 cps vs ~175.6 cps at the surface
    - Dose rates in the mine laboratory: ~1.3 ± 0.3 nSv/h vs ~1.6 ± 0.3 nSv/h across the mine;
- ^{222}Rn concentration ~10 Bq/m³ vs ~ 100 Bq/m³ in the IVB laboratory.

[11] Brede, H.J.; Cosack, M.; Dietze, G.; Gumpert, H.; Guldbakke, S.; Jahr, R.; Kutscha, M.; Schlegel-Bickmann, D.; Schölermann, H. The Braunschweig accelerator facility for fast neutron research: 1: Building design and accelerators. Nuclear Instruments and Methods 1980;169:349-358, doi:https://doi.org/10.1016/0029-554X(80)90928-3.

[12] Ziegler, J.; Ziegler, M.D.; Biersack, J. The Stopping and Range of Ions in Mater. Nuclear Instruments and Methods in Physics Research Section B: Beam Interactions with Materials and Atoms 2010; 268, 1818-1823, doi:10.1016/j.nimb.2010.02.091.

Because the laboratory in the salt mine is not endowed with a facility for biological studies, cells were cultivated for 72 h in tightly capped cell culture flasks on a holder placed within a covered 37 °C water bath, at the air-water interface.

UVB irradiation

To simulate the impact of UVB radiation from sunlight, both independently and in combination with proton radiation on various normal cell lines, a UVB spot source was used (Figure 3-a). This unit employs a 200 W Xenon high-pressure lamp of type Hamamatsu LC8. It is equipped with an optical fiber light guide, a filter package to restrict the spectral range mainly to the UVB spectral range, and a light-shaping diffuser to produce a uniform irradiation field on the sample box, where a typical UV irradiance of 6.6 W/m^2 could be reached, primarily within the 280 nm to 315 nm wavelength range (see Figure 3-b). The irradiances of the UVB spot source were monitored using a UV radiometer, situated at the base of the sample holder. The sample holder inside the irradiation chamber allows the insertion of the sample box in different orientations, and is designed to accommodate up to four slots for exposure, as illustrated in Figure 3-c. The UVB spot source was assembled, characterized, and repeatedly calibrated at the working group 4.11 “Spectroradiometry” at the PTB.

a.

b.

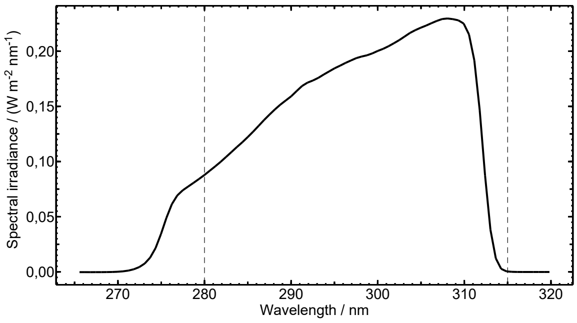

c.

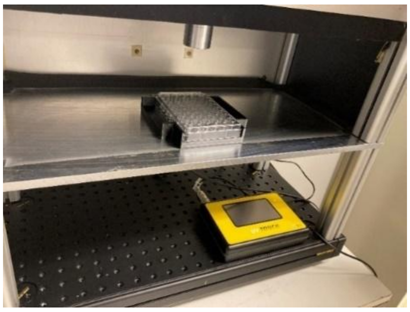

Figure 3. LC8 irradiation unit. UVB spot source unit with irradiation chamber and monitor radiometer (**a**); spectral irradiance distribution of the UVB spot source (**b**); the sample box is inserted into the chamber from the front, and can be orientated in different directions (**c**).

The UVB exposure time is adjustable *via* the LC8 Controller software, enabling the input of specific irradiation durations to regulate the lamp's output. The necessary exposure time t (s) for a given dose H_{UVB} in (J/m^2) is determined by the following formula:

$$t = \frac{H_{UVB}}{E_{UVB}},$$

where E_{UVB} is the actual UVB irradiance in (W/m^2), measured with the monitor radiometer.

Post-exposure investigations

Post-exposure cultivation of cells

(Co)exposed cellular samples and the corresponding controls were diluted in complete culture medium specific for each cell type, and were cultivated at 37°C in 5% CO_2 atmosphere for various tests, as it will be described below.

Cell viability tests

Cellular viability at various time points after the exposure of cells to protons and/or UVB was assessed as number of metabolically active cells using the standard assay of reduction of the tetrazolium compound MTS [3-(4,5-dimethylthiazol-2-yl)-5-(3-carboxymethoxyphenyl)-2-(4-sulfophenyl)-2H-tetrazolium], using the CellTiter 96® AQueous One Solution Cell Proliferation Assay (G3582, Promega Corporation, Madison, WI, USA). Briefly, 10^4 HaCaT cells, 10^4 Hs27 cells, or 3-5 x 10^4 CRL 9855 monocytes were plated in triplicate in a 96-well plate with flat bottom, in 100 µL total volume of complete culture medium. At various time points, 20 µL detection reagent from the kit were added in each well. Cells were further cultivated at 37°C in 5% CO_2 atmosphere until the colorimetric MTS reduction reaction was developed. The incubation time was fixed for each cell type.

In parallel, plasma membrane alteration due to cell death was assessed as lactate dehydrogenase (LDH) release, using the CytoTox 96® Non-Radioactive Cytotoxicity Assay (G1780, Promega Corporation, Madison, WI, USA). Cells were cultivated as described above. At various time points, 50 µL cell-free supernatant were harvested from each sample, and were mixed with 50 µL substrate solution from the kit in a 96-well plate with flat bottom. The colorimetric reaction was allowed to develop for 30 min at room temperature (RT) in the dark, and thereafter, samples were treated with 50 µL stop solution from the above-mentioned kit.

Both colorimetric reactions were measured as optical density (OD) using a Sunrise Tecan ELISA reader (Tecan, Männedorf, Switherland), at 490 nm. In the case of the MTS reduction reaction, the 620 nm reference wavelength was used for subtracting non-specific contributions. The mean OD of control samples in triplicate was used for calculating the effect of irradiation according to the formula: irradiation effect = $\frac{OD\ irradiated\ sample}{mean\ OD\ control}$. Supra unit effects mean activation, while subunit effects inhibition.

DNA damage immunofluorescence study

<u>Hs27 Fibroblasts and HaCat Keratinocytes</u>

The DNA damage inflicted by the exposure of cells to protons and/or UVB was assessed using the γH2AX assay as compared to non-exposed control cells kept in the biology laboratory, according to the following method. Briefly, exposed and control cells in suspension were plated over 22x22 mm^2 coverslips in 35 mm dishes, and were analysed for the γH2AX assay at various time points post-exposure (4 h and 24 h). Cells were fixed for 15 min at RT with paraformaldehyde 3% (F8775, Sigma-Aldrich, Darmstadt, Germany) and sucrose 2% (A2211, Applichem GmbH, Darmstadt, Germany) in phosphate buffered saline (PBS) (18912-014, Gibco, Grand Island, NY, USA), and then were washed once with PBS. Cells were thereafter permeabilized for 10 min with 0.5% Triton X-100 (X100, Merck, Saint Louis, MO, USA) in 100 mM Tris-HCL pH 7.4 (A4263, Applichem GmbH, Darmstadt, Germany) and 50 mM EDTA pH 8 (A4982, AppliChem GmbH, Darmstadt, Germany) in distilled water, were washed again two times with PBS, and were blocked overnight at 7°C with 0.5% bovine albumin (BSA) (A7906, Sigma-Aldrich, Darmstadt, Germany) and 0.2% gelatin from cold water fish (G7041, Sigma-Aldrich, Darmstadt, Germany) in PBS. Samples were then stained with an antibody against histone H2AX (p S139) (NB100-384, Novus Biologicals, Abingdon, UK) in 0.5% BSA and 0.2% gelatin in PBS. After a 90 min-incubation at RT, cells were washed three times with PBS, and were thereafter treated for 90 min at RT with goat anti-rabbit IgG H&L cross-absorbed secondary antibody labeled with Rhodamine Red-X (R-6394, Thermo Fisher Scientific, Waltham, MA, USA) in 0.5% BSA and 0.2% gelatin in PBS. After immunostaining, cells were washed three times with PBS, and were stained with ProLong Gold Antifade Reagent with 4′6-diamidino-2-phenylindole (DAPI) (8961, Cell Signaling Technology Inc, Danvers, MA, USA).

<u>CRL 9855 Monocytes</u>

Following irradiation with protons and/or UVB, human monocytes were immediately returned to a 37°C incubator, and were harvested thereafter at various time points (30 min and 24 h) for the γH2AX assay. H2AX phosphorylation detection was performed using a modification of the aforementioned protocol. Briefly, cells were centrifuged on microscope slides using the Cytospin ROTANTA 460/460R centrifuge (Hettich, Tuttlingen, Germany). All cells were fixed for 15 min at RT with paraformaldehyde 3% (F8775, Sigma-Aldrich, Darmstadt, Germany) and sucrose 2% (A2211, Applichem GmbH, Darmstadt, Germany) in PBS (18912-014, Gibco, Grand Island, NY, USA), and were then triple-washed with PBS. Cells were thereafter permeabilized for 10 min with 0.5% Triton X-100 (X100, Merck, Saint Louis, MO, USA) in 100 Mm Tris-HCl pH 7.4 (A4263, Applichem GmbH, Darmstadt, Germany) and 50 Mm EDTA pH 8 (A4982, AppliChem GmbH, Darmstadt, Germany) in distilled water, washed again three times with PBS, and blocked overnight at 7^{o}C with 0.5% BSA (A7906, Sigma-Aldrich, Darmstadt, Germany) and 0.2% gelatin from cold water fish (G7041, Sigma-Aldrich, Darmstadt, Germany) in PBS. Cells were incubated for 90 min at RT with an antibody against histone H2AX (p S139) (NB100-384, Novus Biologicals, Abingdon, UK) in 0.5% BSA and 0.2% gelatin in PBS, and were then washed three times with PBS. A 90 min incubation at RT with goat anti-rabbit IgG H&L cross-absorbed secondary antibody labelled with Rhodamine Red-X (R-6394, Thermo Fisher Scientific, Waltham, MA, USA) in 0.5% BSA and 0.2% gelatin in PBS followed. After three times washing with PBS, DNA was counterstained with ProLong Gold Antifade Reagent with 4′6-diamidino-2-phenylindole (DAPI) (8961, Cell Signaling Technology Inc, Danvers, MA, USA) and cells were shielded with 22x22 mm coverslips, avoiding air bubbles trapping. To access what percentage of γH2AX foci corresponds to double strand breaks (DSBs), double immunofluorescence was performed by following the affirmation protocol with a difference in staining procedure. Samples were double-stained with an antibody against histone H2AX (p S139) (80312T, Cell Signaling Technology, 3 Trask Lane, Danvers, MA, USA) and an antibody against 53PB1 (88439, Cell Signaling Technology, 3 Trask Lane, Danvers, MA, USA) in 0.5% BSA and 0.2% gelatin in PBS. After a 90 min-incubation at RT, cells were washed three times with PBS and were thereafter treated for 90 min at RT with Anti-mouse IgG (H+L), F(ab')2 Fragment (Alexa Fluor® 488 Conjugate) (4408S, Cell Signaling Technology, 3 Trask Lane, Danvers, MA, USA) and Anti-rabbit IgG (H+L), F(ab') 2 Fragment (Alexa Fluor ® 594 Conjugate) (8889S, Cell Signaling Technology, 3 Trask Lane, Danvers, MA, USA) in 0.5% BSA and 0.2% gelatin in PBS.

At least two independent experiments were conducted for each experimental condition in all cell lines. Microscope slides were analyzed using a Zeiss Axioskop-2 fluorescence microscope (Carl Zeis, Göttingen

Germany) with ISIS software. More than 100 cells/slide were analysed with the JCountPro and JQuantPlus image processing software (courtesy of Dr. Pavel Lobachevsky group, Peter McCallum Institute, Australia)[13].

Gene expression study

Irradiated and non-irradiated controls of HaCaT and Hs27 cells (0.5 x 10^6/sample) were cultivated for 48 h in 6-well plates in a total complete medium volume of 2.5 mL, whilst CRL 9855 monocytes (0.9 x 10^6 cells) were cultivated for 24 h in 24-well plates in 2 mL complete medium. At the end of the cultivation time, the supernatant of the HaCaT and Hs27 cultures was discarded, the adherent cells, presumed to be viable cells, were washed with Dulbecco's phosphate buffered saline (DPBS, D8537 Sigma-Aldrich, Saint Louis, USA), and were finally suspended in 1 mL RiboZol™ RNA Extraction Reagent (N580 Avantor, VWR Funding, Radnor, Pennsylvania, USA). Non-adherent CRL 9855 monocytes were washed by centrifugation with DPBS, and were finally suspended in RiboZol™ RNA Extraction Reagent. All samples in RiboZol were stored frozen at around -18°C at PTB for 7 days at most, being thereafter transported in dry ice to Romania, where samples were stored at -80°C until use.

Gene expression was evaluated by qRT-PCR, as previously described[14]. Total concentration of RNA in RiboZol samples was measured using the Nanodrop 2000 equipment (NanoDrop Technologies, Wilmington, DE, USA), the registered values of the 260/280 nm and 260/230 nm ratios being above 1.8. The RT^2 First Strand Kit (Qiagen, Hilden, Germany) was used for cDNA synthesis. The expression of 84 genes involved in stress and toxicity was evaluated using the RT² Profiler™ PCR Array Human Stress & Toxicity Pathway Finder (PAHS-003Z, Qiagen, Hilden, Germany) (Table 1), and the SYBR Green chemistry on ABI7500 Fast PCR System (Thermo Fisher Scientific, Waltham, MA, USA). The expression level of each gene was normalized to the geometric mean value of 5 housekeeping genes (ACTB, B2M, GAPDH, HPRT1, and RPLP0). In some

[13] Nikitaki Z, Pariset E, Sudar D, Costes SV, Georgakilas AG. In Situ Detection of Complex DNA Damage Using Microscopy: A Rough Road Ahead. Cancers (Basel). 2020;12(11):3288. doi: 10.3390/cancers12113288.
[14] Dobre M, Boscencu R, Neagoe IV, Surcel M, Milanesi E, Manda G. Insight into the Web of Stress Responses Triggered at Gene Expression Level by Porphyrin-PDT in HT29 Human Colon Carcinoma Cells. Pharmaceutics. 2021 7;13(7):1032. doi: 10.3390/pharmaceutics13071032.

cases, relevant housekeeping genes were selected using the RefFinder algorithm[15] out of the five above-mentioned reference genes. Gene expression data were analysed with the RT^2 Profiler PCR Array software package (Qiagen, Hilden, Germany). Gene expression levels were calculated as $2^{-\Delta CT}$ values. Fold change (FC) in gene expression was calculated as the $2^{-\Delta CT}$ values in irradiated samples divided by the $2^{-\Delta CT}$ values in controls[16]. FC values > 1 designate gene over-expression, while FC values <1 gene indicate under-expression. Results were expressed as mean FC ± SD.

Table 1. Stress genes in the RT² Profiler™ PCR Array Human Stress & Toxicity PathwayFinder (PAHS-003Z, Qiagen).

Cell Death	***Apoptosis*** CASP1 (ICE), FAS, MCL1, TNFRSF10A (TRAIL-R), TNFRSF10B (DR5), TNFRSF1A (TNFR1).
	Necrosis FAS, GRB2, PARP1 (ADPRT1), PVR, RIPK1, TNFRSF10A (TRAIL-R), TNFRSF1A (TNFR1), TXNL4B.
	Autophagy ATG12, ATG5, ATG7, BECN1, FAS, ULK1.
DNA Damage & Repair	***Cell Cycle Arrest & Checkpoints*** CDKN1A (p21CIP1, WAF1), CHEK1, CHEK2 (RAD53), DDIT3 (GADD153, CHOP), HUS1, MRE11, NBN, RAD17, RAD9A.
	Other DNA Damage Responses ATM, ATR, DDB2, GADD45A, GADD45G, RAD51, TP53 (p53), XPC.
Unfolded Protein Response	ATF4, ATF6, ATF6B, BBC3 (PUMA), BID, CALR, DDIT3 (GADD153, CHOP), DNAJC3, HSP90AA1, HSP90B1, HSPA4 (HSP70), HSPA5 (GRP78).
Oxidative Stress FTH1, GCLC, GCLM, GSR, GSTP1, HMOX1, NQO1, PRDX1, SQSTM1, TXN, TXNRD1.	**Hypoxia Signaling** ADM, ARNT, BNIP3L, CA9, EPO, HMOX1, LDHA, MMP9, SERPINE1 (PAI-1), SLC2A1, VEGFA.
Inflammatory Response CCL2 (MCP-1), CD40LG, CRP, CXCL8 (IL8), IFNG, IL1A, IL1B, IL6, TLR4, TNF.	**Osmotic Stress** AKR1B1, AQP1, AQP2, AQP4, CFTR, EDN1, HSPA4L (OSP94), NFAT5, SLC5A3.

3 Results

The impact of the co-exposure to energetic protons and UVB radiation of human normal cell lines, Hs27 fibroblasts, HaCaT keratinocytes and CRL 9855 monocytes, was evaluated in terms of cellular viability, the expression changes of stress genes, and DNA damage, as compared to the cellular response to protons or UVB alone.

Cellular viability

The impact of UVB and broad proton beams as single or combined radiations on human normal skin cells (Hs27 fibroblasts and HaCaT keratinocytes) and normal CRL 9855 was investigated using the MTS reduction assay that provides information on the number of metabolically active cells in culture, in conjunction with the LDH release assay that indicates plasma membrane alterations related to cell death by necrosis, necroptosis and late apoptosis.

Human normal Hs27 skin fibroblasts

The impact of various UVB fluences on the viability of human normal Hs27 skin fibroblasts was investigated at 6 h and 24 h post-exposure in terms of MTS reduction and LDH release. The MTS reduction by Hs27 fibroblasts was not affected at 6 h after UVB exposure but decreased following a dose-effect relationship at fluences > 50 J/m^2 at 24 h (Figure 4-a). This effect on MTS reduction was not accompanied by an increase of LDH release (Figure 4-b), indicating that the decrease in the number of metabolically active Hs27 fibroblasts

[15] Xie F, Wang J, Zhang B. RefFinder: a web-based tool for comprehensively analyzing and identifying reference genes. Funct Integr Genomics. 2023;23(2):125. doi: 10.1007/s10142-023-01055-7.

[16] Dobre M, Boscencu R, Neagoe IV, Surcel M, Milanesi E, Manda G. Insight into the Web of Stress Responses Triggered at Gene Expression Level by Porphyrin-PDT in HT29 Human Colon Carcinoma Cells. Pharmaceutics. 2021;13(7):1032. doi: 10.3390/pharmaceutics13071032.

was not due to cell death accompanied by alterations of the plasma membrane integrity. In fact, the slight decrease of LDH release, which paralleled the decrease of MTS reduction at fluences over 100 J/m^2, indicated the decrease of the spontaneous (basal) LDH release due to a lower number of metabolically active cells in culture.

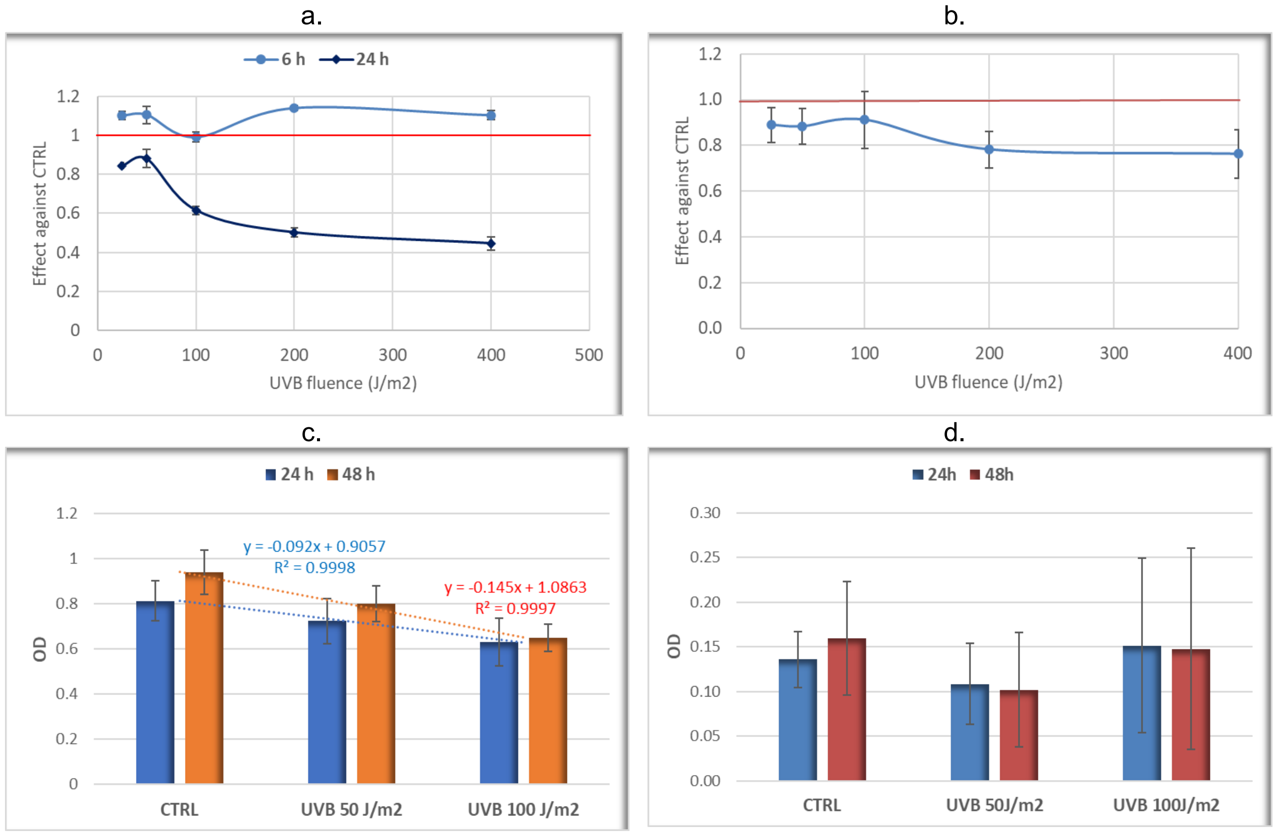

Figure 4. Viability of human normal Hs27 skin fibroblasts exposed to UVB. The effect of UVB exposure was calculated as OD of exposed samples divided by the mean OD value of unexposed control cells. **a.** MTS reduction by cells exposed to various UVB fluences, assessed at 6 h and 24 h post-exposure in triplicate samples (mean effect of UVB exposure ± SEM). The red line designates the unit effect (no effect). **b.** LDH release by cells exposed to various UVB fluences, assessed at 24 h post-exposure in triplicate samples (mean effect of UVB exposure ± SEM). The red line designates the unit effect (no effect); **c.** MTS reduction by cells exposed to UVB fluences of 50 J/m^2 and 100 J/m^2, assessed at 24 h and 48 h post-exposure (mean OD ± SD for 7 independent experiments); **d.** LDH release by cells exposed to UVB fluences of 50 J/m^2 and 100 J/m^2, assessed at 24 h and 48 h post-exposure (mean OD ± SD for 7 independent experiments). Trendlines at 24 h (blue line) and 48 h (red line), and their equations are presented.

We further investigated in more detail, in 7 independent experiments, the effect of UVB at fluences of 50 J/m^2 and 100 J/m^2 on the viability of Hs27 fibroblasts at 24 h and 48 h post-exposure. MTS reduction decreased following a dose-effect relationship (Figure 4-c). While 100 J/m^2 UVB decreased MTS reduction both at 24 h and 48 h after exposure ($p<0.05$), 50 J/m^2 UVB inflicted damage slowly, the changes *vs* CTRL being significant only at 48 h ($p<0.05$). The effects of 50 and 100 J/m^2 were statistically different both at 24 h ($p<0.01$) and 48 h ($p<0.001$). Of note is that cells exposed to 100 J/m^2 did not proliferate anymore between 24 h and 48 h post-exposure to UVB, as no difference in MTS reduction was registered. The decreased MTS reduction was not accompanied by significant changes of LDH release (Figure 4-d), indicating that cells exposed to the investigated UVB fluences did not die by massive necrosis/necroptosis or late apoptosis that involve alteration of the plasma membrane integrity.

When Hs27 fibroblasts were exposed to protons of various doses (0.25 – 0.5 – 1 Gy), no significant changes of MTS reduction at 24 h after irradiation were detected, neither when cells were placed in the bottom plate or in the upper dish (Figure 5-a). Exposure of cells to 0.5 Gy protons did not significantly alter the viability of fibroblasts in terms of MTS reduction (Figure 5-b) or LDH release (Figure 5-c). Altogether, experimental data show that protons did not alter the viability of Hs27 fibroblasts in the investigated dose range, no matter if cells were exposed to protons in the bottom plate or in the upper dish.

A more detailed analysis was performed on Hs27 fibroblasts exposed to 0.5 Gy protons in the bottom plate. Two controls were used for comparison: a control kept in the biology laboratory (CTRL), also used as a reference for UVB exposure, and a control in the irradiation facility (IrrCTRL). Control cells kept in the irradiation room (IrrCTRL), had a small decrease in MTS reduction compared to the laboratory CTRL (Figure 5-b), indicating that they might have been exposed and slightly harmed by the background radiation (14 mGy per Gy of proton dose delivered to cells). The exposure of cells to 0.5 Gy protons (Figure 5-b) decreased the MTS reduction as compared to CTRL, especially at 48 h post-exposure ($p<0.05$), but not at 24 h when cells appeared to be mostly affected by the background radiation. Altogether, experimental data indicated that 0.5 Gy protons inflicted a slight reduction of the number of metabolically active Hs27 fibroblasts at 48 h after their exposure, and that cells seemed to be slightly affected also by the background radiation in the irradiation facility.

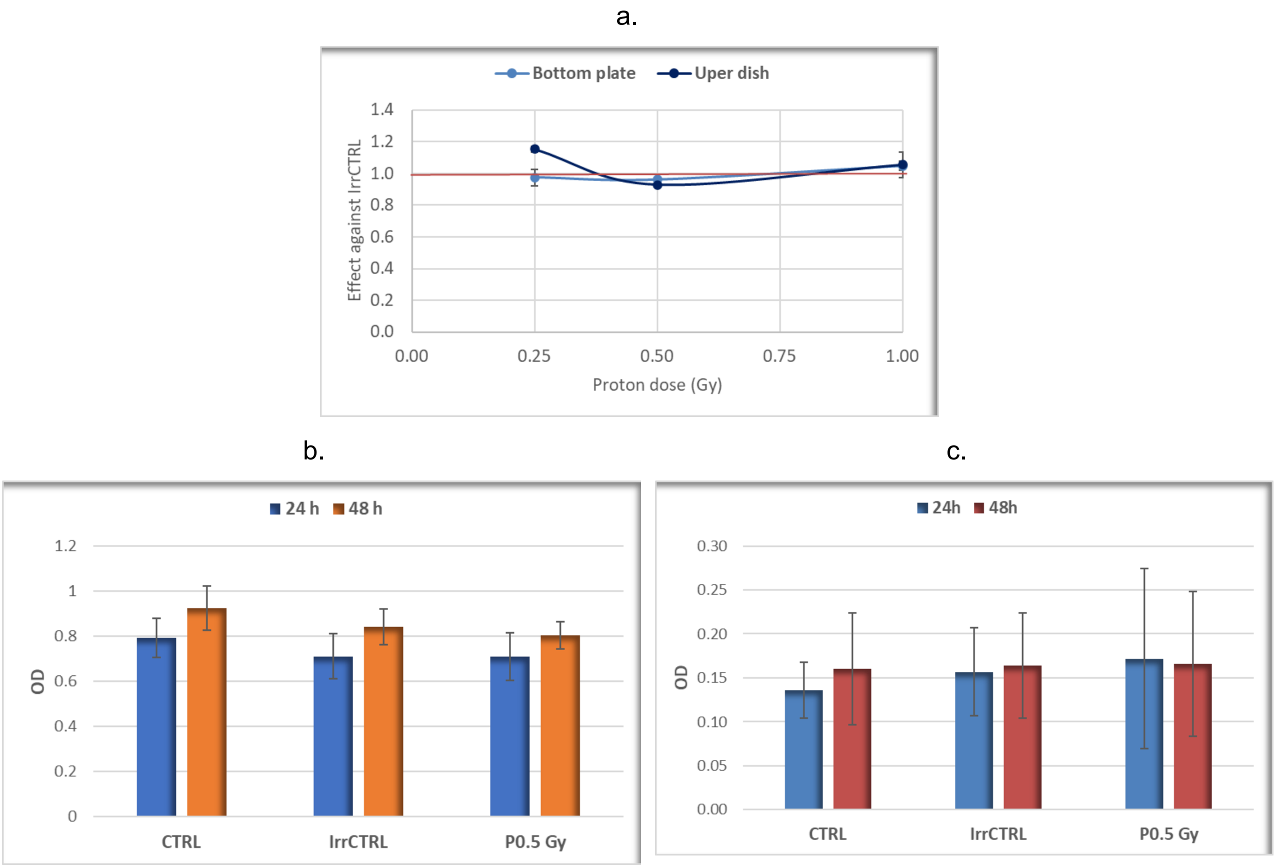

Figure 5. MTS reduction by human normal Hs27 skin fibroblasts exposed protons. Cells were placed either in the bottom plate or in the upper dish (Figure 2). The effect of proton exposure was calculated as OD of exposed samples divided by the mean OD value of unexposed control cells kept in the irradiation facility (IrrCTRL). **a.** Cells exposed to various doses of protons, and analysed against the IrrCTRL at 24 h post-exposure on triplicate samples (mean effect of proton exposure ± SEM). The red line designates the unit effect (no effect); **b.** MTS reduction at 24 h and 48 h after exposure of cells to 0.5 Gy protons (mean OD ± SD for 7 independent experiments); **c.** LDH release at 24 h and 48 h after exposure of cells to 0.5 Gy protons (mean OD ± SD for 7 independent experiments)

Finally, the impact of the co-exposure of Hs27 fibroblasts to protons and UVB was analysed. In four independent experiments, we investigated the viability of Hs27 fibroblasts exposed first to 0.5 Gy protons and then, within approximately. 20 min, to 50 J/m^2 or 100 J/m^2 UVB (Figure 6).

In this set of experiments, protons decreased MTS reduction at 48 h, as compared with both the CTRL and IrrCTRL samples ($p<0.05$), but not earlier, at 24 h post-exposure (Figure 6-a). The decrease in MTS reduction was not accompanied by an increase of LDH release (Figure 6-b), indicating that the decrease of the number of metabolically active Hs27 fibroblasts was not due to significant cell death with alteration of the plasma membrane.

While UVB 50 J/m^2 decreased MTS reduction only late, at 48 h ($p<0.05$), UVB 100 J/m^2 affected MTS reduction both at 24 h and 48 h as compared to CTRL ($p<0.01$) (Figure 6-a). The investigated UVB fluences exerted different effects on Hs27 fibroblasts at 24 h ($p<0.01$) and 48 h ($p<0.001$) post-exposure. Likewise, in the case of UVB exposure, the LDH released by Hs27 fibroblasts did not change significantly compared to CTRL (Figure 6-b), suggesting that the reduction of metabolically active cells was not due to significant cell death.

The MTS reduction by co-exposed fibroblasts was significantly lower as compared to the effects of protons or UVB alone (Figure 6). Thus, the exposure of cells to 0.5 Gy protons and thereafter to 50 J/m^2 UVB induced a slight decrease of MTS reduction at 24 h as compared to protons alone ($p<0.05$, effect against protons at 24 h: 0.92 ± 0.03), and as compared to UVB 50 J/m^2 alone ($p_{one\ tail}<0.05$, effect against UVB 50 J/m^2 at 24 h = 0.91 ± 0.06). This decrease was more pronounced at 48 h after co-exposure, both as compared to protons alone ($p<0.001$, effect against protons at 48 h: 0.88 ± 0.01) and UVB alone ($p<0.05$, effect against UVB 50 J/m^2 at 48 h = 0.85 ± 0.05) alone. Altogether, results indicated a persistent synergistic effect of protons and UVB in the co-exposure scenario.

When cells were co-exposed to 0.5 Gy protons and a higher UVB fluence of 100 J/m^2, a marked decrease in MTS reduction was registered at 24 h and 48 h after irradiation both against protons alone ($p<0.05$, effect against protons at 24 h: 0.73 ± 0.06, effect against protons at 48 h: 0.71 ± 0.10) and UVB alone ($p<0.05$, effect against UVB 100 J/m2 at 24 h: 0.86 ± 0.06, effect against UVB 100 J/m^2 at 48 h: 0.85 ± 0.09) (Figure 6), indicating again a marked synergistic effect.

a. b.

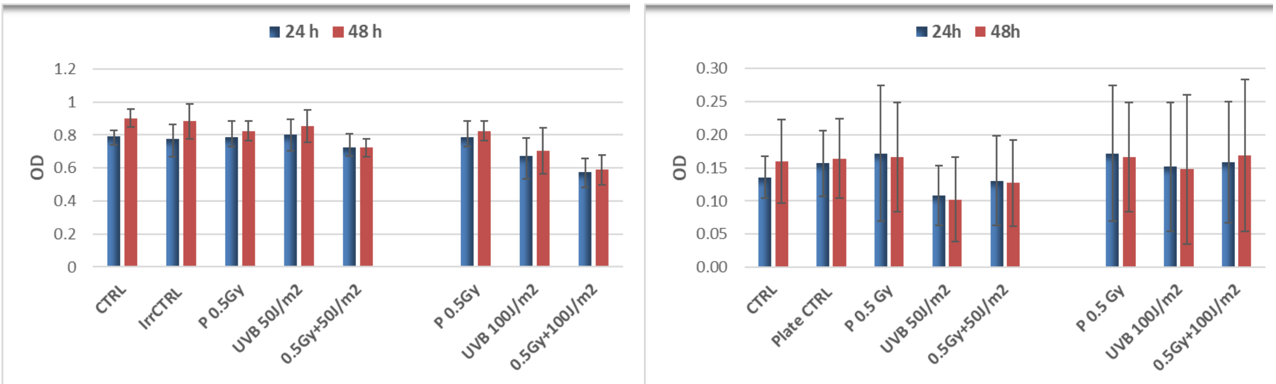

Figure 6. MTS reduction by human normal Hs27 fibroblasts at 24 h and 48 h after exposure to 0.5 Gy protons, and thereafter, within approx. 20 min, to UVB (50 J/m^2 or 100 J/m^2). Results are presented as mean OD ± SD for 4 independent experiments. **a.** MTs reduction; **b.** LDH release. CTRL-laboratory control, irrCTRL-control cells kept in the proton irradiation facility.

Concluding, UVB and protons exerted a synergistic action on the ability of Hs27 fibroblasts to reduce MTS, indicating a decrease in the number of metabolically active cells due to the combined challenges. This decrease of MTS reduction was not due to significant cell death.

Human normal HaCaT keratinocytes

UVB exposure of human normal HaCaT keratinocytes had major effects on MTS reduction at 6 h post-exposure, but drastically decreased MTS reduction at 24 h after irradiation at fluences ≥ 50 J/m^2 (Figure 7-a), with a significant increase of LDH release at fluences ≥ 100 J/m^2 (Figure 7-b). Results indicate that UVB decreased slowly the number of metabolically active cells within 24 h post-exposure, and this was partly due to cell death with alterations of the plasma membrane.

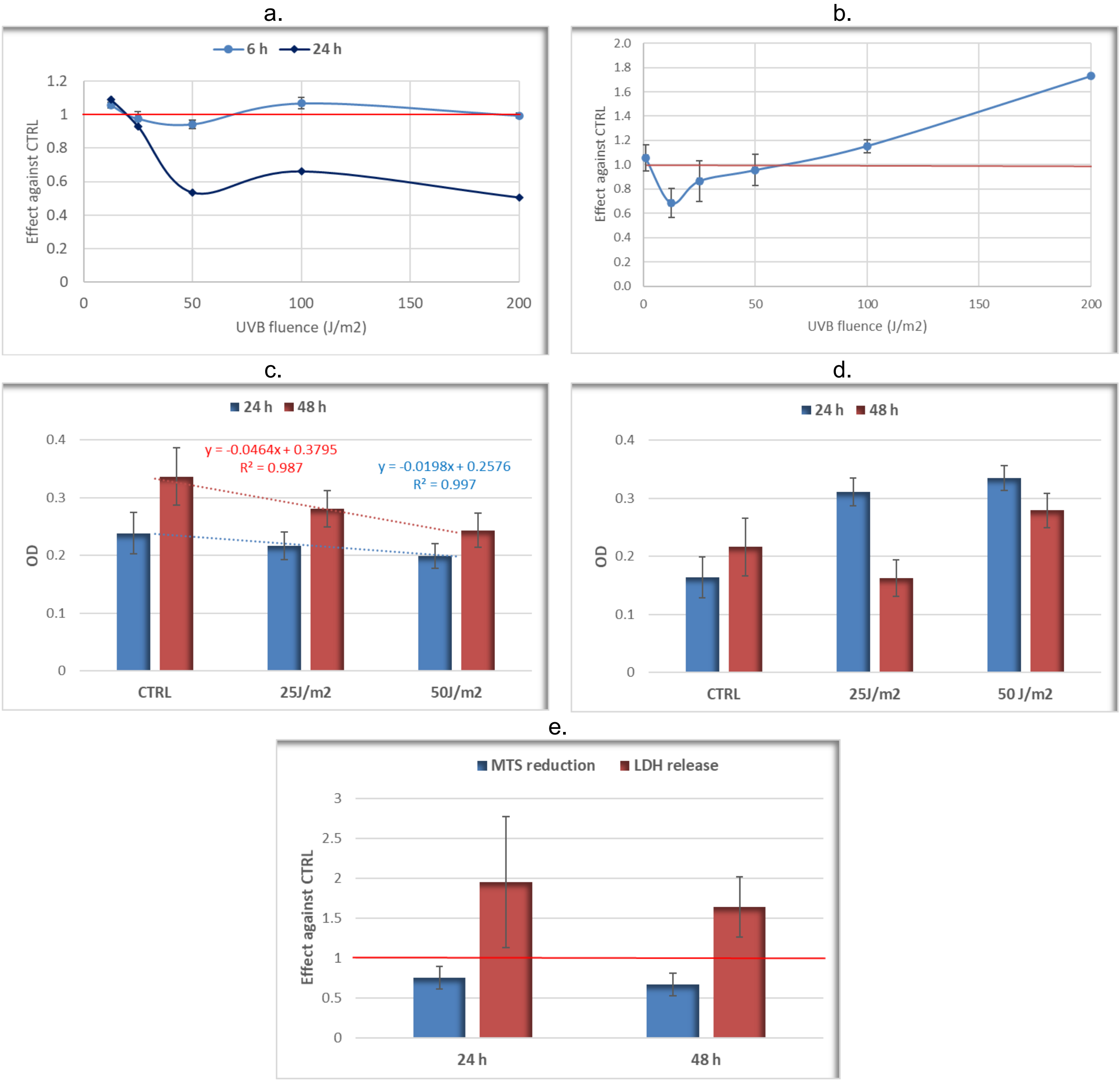

Figure 7. Viability of human normal HaCaT keratinocytes exposed to UVB. The effect of UVB exposure was calculated as OD of exposed samples divided by the mean OD value of unexposed control cells (CTRL). **a.** MTS reduction by cells exposed to various UVB fluences, assessed at 6 h and 24 h post-exposure in triplicate samples (mean effect of UVB exposure ± SEM). The red line designates the unit effect (no effect); **b.** LDH release by cells exposed to various UVB fluences, assessed at 24 h post-exposure in triplicate samples (mean effect of UVB exposure ± SEM). The red line designates the unit effect (no effect); **c.** MTS reduction by cells exposed to UVB fluences of 25 J/m^2 and 50 J/m^2, assessed at 24 h and 48 h (mean OD ± SD for 3 independent experiments). Trendlines at 24 h (blue line) and 48 h (red line), and their equations are presented; **d.** LDH release by cells exposed to UVB fluences of 25 J/m^2 and 50 J/m^2, assessed at 24 h and 48 h (mean OD ± SD for 3 independent experiments). Trendlines at 24 h (blue line) and 48 h (red line), and their equations are

presented; **e.** MTS reduction by cells exposed to 50 J/m^2 UVB, assessed at 24 h and 48 h post-exposure (mean OD ± SD for 7 independent experiments).

A more detailed analysis of 3 independent experiments on the effect of UVB 25 J/m^2 and 50 J/m^2 (Figure 7-c) showed a dose-effect relationship of MTS reduction by HaCaT keratinocytes both at 24 h and 48 h after exposure ($p<0.05$). The decrease of MTS reduction was accompanied by a fluence-independent increase of LDH release at 24 h, which persisted also at 48 h only in the case of cells exposed to 50 J/m^2 UVB (Figure 7-d), indicating that this higher fluence was persistently cytotoxic, as shown also in Figure 7-d with data from 7 independent experiments.

When HaCaT keratinocytes were exposed to protons in the dose range of (0.25 – 1) Gy no significant changes in MTS reduction were registered (Figure 8).

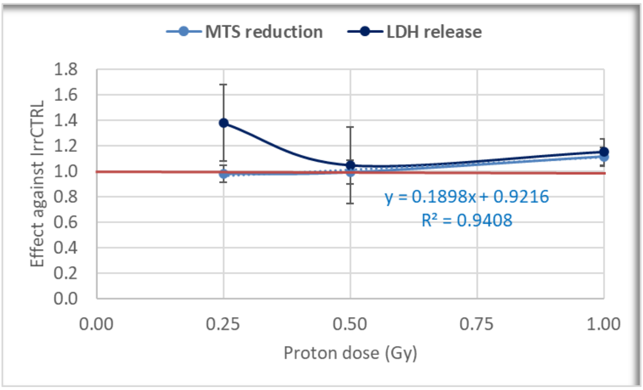

Figure 8. MTS reduction by human normal HaCaT keratinocytes exposed to various doses of protons. Results are presented as the mean effect of proton exposure ± SD for 3 independent experiments. The effect of proton exposure was calculated as OD of exposed samples divided by the mean OD value of unexposed control cells kept in the irradiation facility (IrrCTRL). The red line designates the unit effect (no effect).

The impact of the exposure of HaCaT keratinocytes to 0.5 Gy protons first, and then, within approximately. 20 min, to 25 J/m^2 or 50 J/m^2 UVB was analysed in 3 independent experiments.

In this set of co-exposure experiments, protons alone did not alter at 24 h or 48 h MTS reduction as compared with either CTRL or IrrCTRL, whilst UVB 25 J/m^2 or 50 J/m^2 decreased MTS reduction at 48 h in a fluence-effect relationship (UVB 25 J/m^2 *vs* 50 J/m^2: $p_{one\ tail} < 0.05$) (Figure 9-a).

The co-exposure of cells to 0.5 Gy protons and 25 J/m^2 UVB did not induce changes of MTS reduction at 24 h compared to protons or UVB alone, but induced at decrease in MTS reduction at 48 h post-exposure compared to protons alone ($p_{one\ tail} <0.05$, effect against protons = 0.74 ± 0.14), but not compared to UVB alone (Figure 9-a). This effect of the co-exposure was therefore due to UVB exposure.

When the UVB fluence of 50 J/m^2 was used in the co-exposure setting with 0.5 Gy protons (Figure 9-a), MTS reduction by HaCaT keratinocytes was significantly lower in co-exposed samples at 24 h, either compared to protons alone ($p<0.05$, effect against protons = 0.79 ± 0.06) or to UVB alone ($p<0.01$, effect = 0.90 ± 0.11), indicating a synergistic effect. At 48 h, the MTS reduction by co-exposed cells was significantly lower than in cells exposed to protons alone ($p<0.01$, effect against protons = 0.64 ± 0.04), but was comparable to the data registered in samples exposed to UVB alone (Figure 9-a), indicating that the effect at 48 h was mainly due to UVB exposure.

LDH release by HaCaT cells co-exposed to 0.5 Gy protons and 25 J/m^2 or 50 J/m^2 was increased (mean effect > 1) in both UVB irradiation settings (Figure 9-b). While this increase was due to 50 J/m^2 UVB exposure in the 0.5 Gy + 50 J/m^2 setting, a synergic effect was registered in the 0.5 Gy + 25 J/m^2 setting, considering that protons or 25 J/m^2 UVB applied as single challenges did not significantly alter LDH release as compared to CTRL, whilst in co-exposed cells a tendency of intensified LDH release was registered (Figure 9-b).

a. b.

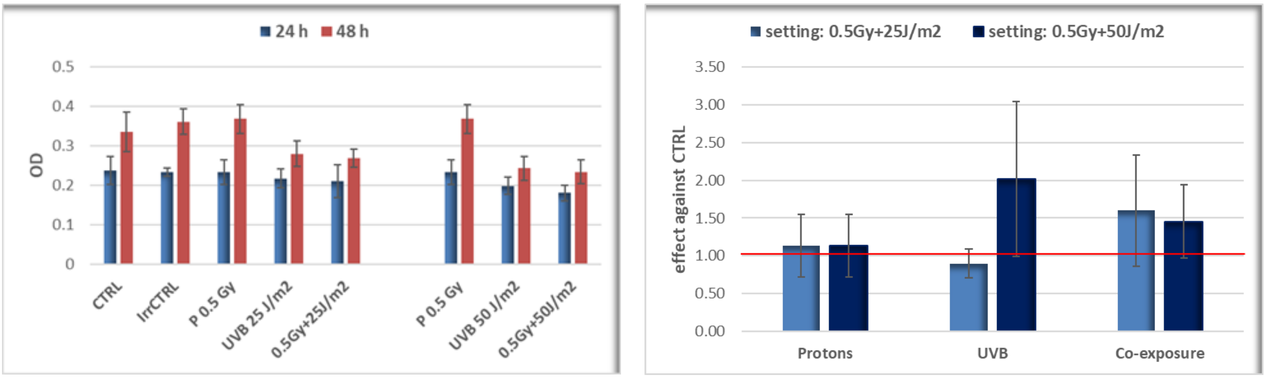

Figure 9. MTS reduction by human normal HaCaT keratinocytes after exposure to 0.5 Gy protons, and thereafter, within approximately. 20 min, to UVB (25 J/m^2 or 50 J/m^2). **a.** MTS reduction at 24 h and 48 h post-exposure (mean OD ± SD for 3 independent experiments); **b.** LDH release at 48 h after post-exposure (mean effect ± SD for 3 independent experiments). The effect of (co)exposure was calculated as OD of (co)exposed samples divided by the mean OD value of unexposed control cells (CTRL). The red line designates the unit effect (no effect). CTRL-laboratory control, irrCTRL-control cells kept in the proton irradiation facility.

Human normal CRL 9855 monocytes

Exposure of human CRL 9855 monocytes to UVB drastically decreased the MTS reduction at 24 h after the exposure of cells, 50 J/m^2 being the first investigated fluence at which a significant effect (effect < 0.8) was registered (Figure 10-a).

While only a slight decrease in MTS reduction was triggered by 0.25 Gy protons, 0.5 Gy protons induced a stronger effect in term of decrease of metabolically active cells (**Figure 10-b**).

a. b.

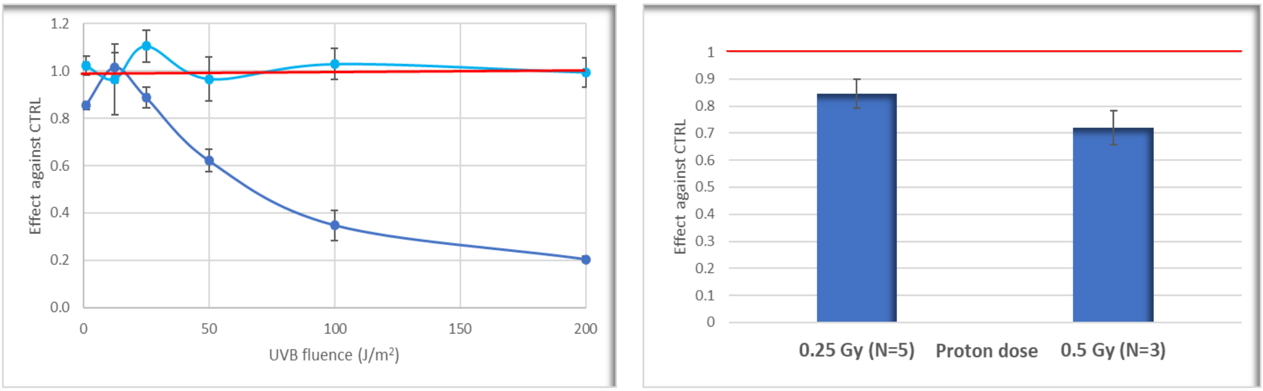

Figure 10. The effect of either UVB (**a**) or proton (**b**) irradiation on the MTS reduction by normal CRL 9855 monocytes. The effect of proton exposure was calculated as OD of exposed samples divided by the mean OD value of unexposed control cells kept in the biology laboratory (CTRL). Results are presented as mean exposure effect ± SEM (a. triplicate samples) or as mean exposure effect ± SD (b. 3-5 independent experiments).

The co-exposure of CRL9855 monocytes to 0.5 Gy protons, and, approx. 20 min thereafter, to 50 J/m2 UVB induced at 24 h post-exposure a marked decrease of MTS reduction that was due to UVB exposure. While UVB alone decreased to approx. 40% MTS reduction, protons alone in the co-exposure experiments did not have a notable effect (Figure 11-a). The decrease of MTS reduction was not accompanied by an increase of LDH release, indicating that the decrease of metabolically active cells by the UVB exposure was not due to cell death with alteration of the plasma membrane integrity.

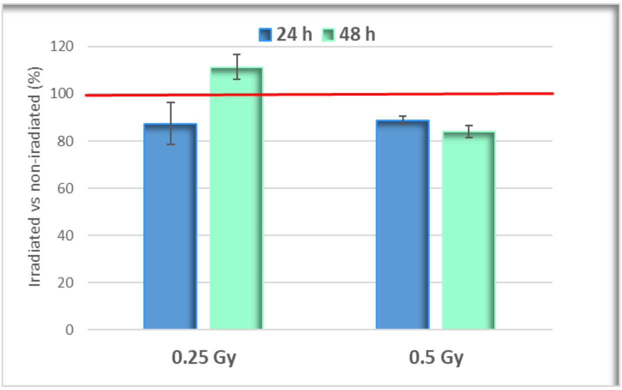

Figure 11. MTS reduction by human normal CRL 9855 monocytes at 24 h after exposure to 0.5 Gy protons, and, within approx. 20 min thereafter, to 50 J/m^2 UVB. The effect of exposure was calculated as OD of exposed samples divided by the mean OD value of unexposed control cells (CTRL). The red line designates the unit effect (no effect). CTRL-laboratory control.

Stress gene expression

Late stress responses

The expression changes of stress genes were quantitatively investigated by qRT-PCR using a pathway-focused array in Hs27 fibroblasts, HaCaT keratinocytes, and CRL 9855 monocytes exposed to 0.5 Gy protons or 50 J/m^2 UVB as single radiations, or co-exposed first to protons and, within approx. 20 min thereafter, to UVB at the above-mentioned doses. Only adherent Hs27 and HaCaT cells, presumably living cells, were investigated, while, in the case of non-adherent CRL 9855 monocytes, all cells, both living and dead, were analysed. Late events registered at 48 h for fibroblasts and keratinocytes, and at 24 h for non-adherent monocytes, were investigated as persistent stress responses. Gene expression results were expressed as “fold change” (FC) relative to the control kept in the biology laboratory (CTRL). Genes with FC values > 1.5 were significantly up-regulated, while genes with FC values < 0.7 were significantly down-regulated.

Hs27 fibroblasts

Exposure of Hs27 fibroblasts to protons or to UVB triggered persistent DNA damage, mirrored at 48 h by the up-regulation of the radiation-sensitive gene HUS1, involved in cell cycle arrest in response to DNA damage[17], and of the XPC gene, involved in DNA damage sensing and DNA binding[18] (Figures 12-a and 12-b). Specifically for cells exposed to protons, the cell cycle arrest gene CDKN1A[19] was found up-regulated (Figure 12-a), complementing the action of HUS1. Meanwhile, the DNA damage sensor MRE11A was up-regulated in cells exposed to UVB (Figure 12-b), complementing the effect of XPC involved in DNA damage recognition[20]. Interestingly, the GADD45G gene, involved in cell cycle arrest for DNA damage repair[21], was down-regulated both in proton and UVB exposures. The DNA damage response registered at 48 h post-exposure to protons or UVB applied as a single radiation was accompanied by the up-regulation of the FAS gene (Figure 12-a,b), involved in receptor-mediated cell death[22].

When Hs27 fibroblasts were co-exposed to 0.5 Gy protons and 50 J/m^2 UVB, a broader pattern of gene expression changes was evidenced (Figure 12-c) as compared to the patterns found when cells were exposed

[17] Parrilla-Castellar ER, Arlander SJ, Karnitz L. Dial 9-1-1 for DNA damage: the Rad9-Hus1-Rad1 (9-1-1) clamp complex. DNA Repair (Amst). 2004;3(8-9):1009-14. doi: 10.1016/j.dnarep.2004.03.032.
[18] Zebian A, El-Dor M, Shaito A, Mazurier F, Rezvani HR, Zibara K. XPC multifaceted roles beyond DNA damage repair: p53-dependent and p53-independent functions of XPC in cell fate decisions. Mutat Res Rev Mutat Res. 2022;789:108400. doi: 10.1016/j.mrrev.2021.108400.
[19] Engeland K. Cell cycle regulation: p53-p21-RB signaling. Cell Death Differ. 2022;29(5):946-960. doi: 10.10
[20] Melis JP, Luijten M, Mullenders LH, van Steeg H. The role of XPC: implications in cancer and oxidative DNA damage. Mutat Res. 2011;728(3):107-17. doi: 10.1016/j.mrrev.2011.07.001.
[21] Palomer X, Salvador JM, Griñán-Ferré C, Barroso E, Pallàs M, Vázquez-Carrera M. GADD45A: With or without you. Med Res Rev. 2024;44(4):1375-1403. doi: 10.1002/med.22015.
[22] Sartorius U, Schmitz I, Krammer PH. Molecular mechanisms of death-receptor-mediated apoptosis. Chembiochem. 2001 Jan 8;2(1):20-9. doi: 10.1002/1439-7633(20010105)2:1<20::AID-CBIC20>3.0.CO;2-X.

solely to protons (Figure 12-a) or to UVB (Figure 12-b). For instance, while GADD45G was down-regulated in all the investigated irradiation settings, only in the co-exposure scenario GADD45A was found to be up-regulated, indicating a prolongation of the GADD45-mediated responses in co-exposed fibroblasts, in addition to CDKN1A and HUS1 as cell cycle blockers. XPC was up-regulated no matter if cells were exposed only to protons (Figure 12-a) or to UVB (Figure 12-b), or were subjected to combined radiations (Figure 12-c). This intensification of DNA damage sensing was complemented by the up-regulation of the ATM gene (DNA damage sensor[23]) in the co-exposure setting (Figure 12-c). In addition, only the co-exposure of cells to protons and UVB induced the up-regulation of DDB2, a gene involved in the repair of ultraviolet light-damaged DNA[24]. As in the case of single stressor exposure (Figures 12-a,b), receptor-mediated cellular death was registered in co-exposed cells, but more genes corresponding to this pathway were found upregulated in addition to FAS in the co-exposure scenario, such as TNFRSF10A and 10B[25] (Figure 12-c).

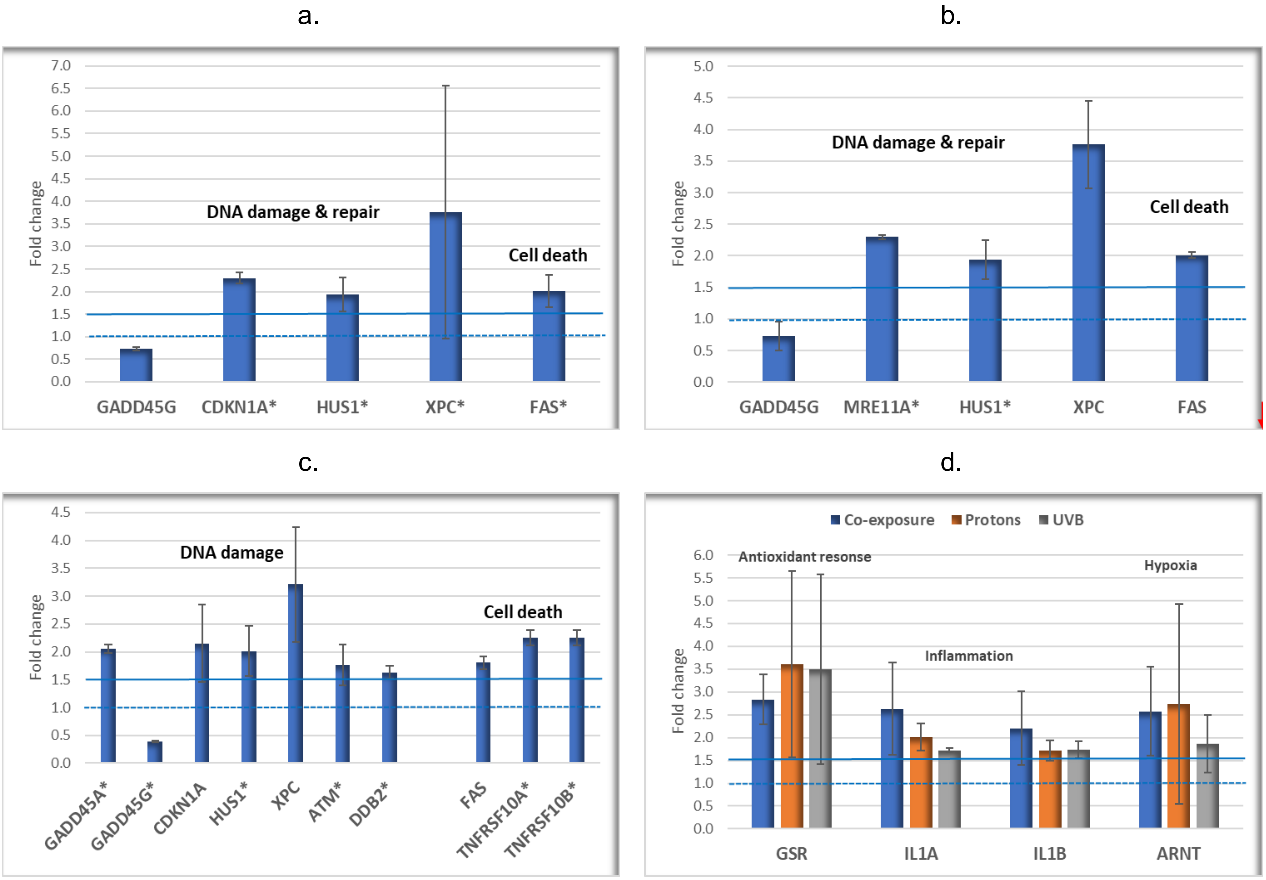

Figure 12. Stress genes with modified expression in human normal Hs27 fibroblasts exposed to 0.5 Gy protons or to 50 J/m^2 UVB applied as single stressors, or combined (proton irradiation followed by UVB exposure within approx. 20 min). Genes with mean fold change > 1.5 (gene up-regulation) or < 0.67 (gene down-regulation) were represented as mean value ± SD in 3 independent experiments. Genes with a significant fold change value in 2 out of 3 experiments and no significant effect in the third experiment were marked with *. The blue line is the low threshold for significant gene up-regulation, while the dashed blue line corresponds to "the no effect" case for evidencing gene down-regulation. **a.** DNA damage & repair genes, and cell death genes in

[23] Baretic D, Maia de Oliveira T, Niess M, Wan P, Pollard H, Johnson CM, Truman C, McCall E, Fisher D, Williams R, Phillips C. Structural insights into the critical DNA damage sensors DNA-PKcs, ATM and ATR. Prog Biophys Mol Biol. 2019;147:4-16. doi: 10.1016/j.pbiomolbio.2019.06.003.
[24] Scrima A, Konícková R, Czyzewski BK, Kawasaki Y, Jeffrey PD, Groisman R, Nakatani Y, Iwai S, Pavletich NP, Thomä NH. Structural basis of UV DNA-damage recognition by the DDB1-DDB2 complex. Cell. 2008 Dec 26;135(7):1213-23. doi: 10.1016/j.cell.2008.10.045.
[25] Gough P, Myles IA. Tumor Necrosis Factor Receptors: Pleiotropic Signaling Complexes and Their Differential Effects. Front Immunol. 2020;11:585880. doi: 10.3389/fimmu.2020.585880.

Hs27 fibroblasts exposed to protons; **b.** DNA damage &repair genes, and death genes in Hs27 fibroblasts exposed to UVB; **c.** DNA damage & repair genes, and cell death genes in Hs27 fibroblasts co-exposed to protons and UVB; d. other stress genes related to antioxidant response, inflammation, and hypoxia response in Hs27 fibroblasts exposed to protons or UVB, or co-exposed to combined radiations.

Several other stress genes were found up-regulated at 48 h after exposure of Hs27 fibroblasts to protons, UVB, or to combined radiations (Figure 12-d). These genes are involved in cellular responses to oxidative stress (GSR[26]), hypoxia (ARNT[27]), and inflammation (IL1A and IL1B[28]). There was no statistical difference regarding the expression changes of common genes among irradiation settings, indicating that radiation effects were not additive with respect to the stress response mediated by the genes presented in Figure 12-d.

Altogether, gene expression results point to a more active DNA damage response (DDR) in fibroblasts co-exposed to protons and UVB compared to the single stressor scenario, possibly due to more profound DNA damage leading to increased commitment to receptor-mediated cell death of co-exposed adhered (presumably living) cells. Fibroblasts elicited various other cytoprotective stress responses, like antioxidant, inflammatory, and hypoxia responses, to counteract the deleterious action of protons and UVB, applied either alone or in combination. According to the gene expression data, co-exposed cells were not protected more than cells exposed to protons or UVB alone regarding antioxidant, inflammatory and hypoxia responses, probably accounting for their increased susceptibility to receptor-mediated death.

HaCaT keratinocytes

Exposure of HaCaT keratinocytes to 0.5 Gy protons (Figure 13-a) elicited at 48 h after irradiation the up-regulation of several genes involved in the DNA damage response (ATM, encoding a DNA damage sensor[29]; CHEK1, encoding a key serine/threonine kinase in the cell cycle checkpoint response[30]; DDB2, encoding the smaller subunit of a heterodimeric protein complex that participates in nucleotide excision repair (NER)[31]. XPC, a DNA damage sensor involved in NER[32] was as well up-regulated (XPC FC: 7.20 ± 8.72), reinforcing the sensing potential of ATM. In turn, other genes involved in the DNA damage response, such as GADD45A and CHEK2, both involved in cell cycle arrest and DNA damage repair[33,34,] were found down-regulated. The down-regulation of the TNFRSF10A gene[35] indicated that keratinocytes exposed to protons have a lower susceptibility of receptor-mediated cell death.

When HaCaT keratinocytes were expose to 50 J/m^2 UVB (Figure 13-b), DDB2 and XPC (XPC FC: 6.30 ± 8.03) were up-regulated, as in the case of cells irradiated with protons (Figure 13-a), indicating an active DNA damage response at 48 h post-exposure to UVB. Meanwhile, several other genes involved in the DNA damage response were down-regulated, such as GADD45A/B and CHEK2, as found also in the case of proton exposure (Figure 13-a). The RAD9A gene involved in cell cycle arrest[36] was found down-regulated specifically in the UVB exposure setting. Moreover, the UVB-specific up-regulation of CASP1, which encodes a caspase

[26] Hayes JD, Dinkova-Kostova AT, Tew KD. Oxidative Stress in Cancer. Cancer Cell. 2020;38(2):167-197. doi: 10.1016/j.ccell.2020.06.001.
[27] Habano W, Miura T, Terashima J, Ozawa S. Aryl hydrocarbon receptor as a DNA methylation reader in the stress response pathway. Toxicology. 2022;470:153154. doi: 10.1016/j.tox.2022.153154.
[28] Goshen I, Yirmiya R. Interleukin-1 (IL-1): a central regulator of stress responses. Front Neuroendocrinol. 2009;30(1):30-45. doi: 10.1016/j.yfrne.2008.10.001.
[29] Maréchal A, Zou L. DNA damage sensing by the ATM and ATR kinases. Cold Spring Harb Perspect Biol. 2013;5(9):a012716. doi: 10.1101/cshperspect.a012716.
[30] Patil M, Pabla N, Dong Z. Checkpoint kinase 1 in DNA damage response and cell cycle regulation. Cell Mol Life Sci. 2013;70(21):4009-21. doi: 10.1007/s00018-013-1307-3.
[31] Stoyanova T, Roy N, Kopanja D, Bagchi S, Raychaudhuri P. DDB2 decides cell fate following DNA damage. Proc Natl Acad Sci U S A. 2009;106(26):10690-5. doi: 10.1073/pnas.0812254106.
[32] Zebian A, Shaito A, Mazurier F, Rezvani HR, Zibara K. XPC beyond nucleotide excision repair and skin cancers. Mutat Res Rev Mutat Res. 2019;782:108286. doi: 10.1016/j.mrrev.2019.108286.
[33] Wingert S, Thalheimer FB, Haetscher N, Rehage M, Schroeder T, Rieger MA. DNA-damage response gene GADD45A induces differentiation in hematopoietic stem cells without inhibiting cell cycle or survival. Stem Cells. 2016;34(3):699-710. doi: 10.1002/stem.2282.
[34] van Jaarsveld MTM, Deng D, Ordoñez-Rueda D, Paulsen M, Wiemer EAC, Zi Z. Cell-type-specific role of CHK2 in mediating DNA damage-induced G2 cell cycle arrest. Oncogenesis. 2020;9(3):35. doi: 10.1038/s41389-020-0219-y.
[35] Montinaro A, Walczak H. Harnessing TRAIL-induced cell death for cancer therapy: a long walk with thrilling discoveries. Cell Death Differ. 2023;30(2):237-249. doi: 10.1038/s41418-022-01059-z.
[36] Hwang BJ, Gonzales R, Corzine S, Stenson E, Pidugu L, Lu AL. DNA binding by the Rad9A subunit of the Rad9-Rad1-Hus1 complex. PLoS One. 2022;17(8):e0272645. doi: 10.1371/journal.pone.0272645.

involved in pyroptotic cell death mediated by inflammatory cytokines[37], was registered. The TNFRSF10A/B genes were down-regulated in cells exposed to UVB, as found also in cells irradiated with protons (Figure 13-a), indicating a lower susceptibility of cells to receptor-mediated cell death.

The pattern of stress genes related to DNA damage and cell death up-regulated in HaCaT keratinocytes co-exposed to protons and UVB (Figure 13-c) recapitulate partly the pattern inflicted by protons (Figure 13-a) or by UVB (Figure 13-b). Thus, ATM and DDB2 were up-regulated in co-exposed cells, as they were in proton-irradiated keratinocytes, while CASP1 was up-regulated in co-exposed cells, as it was in UVB-exposed cells (Figure 13-b). ATR was up-regulated only in co-exposed cells, reinforcing the DNA breaks sensing of ATM and XPC (XPC FC: 7.96 ± 10.94). In turn, CHEK2 and GADD45 genes were down-regulated both in co-exposed, and proton (Figure 13-a) or UVB-irradiated cells (Figure 13-b). Meanwhile, RAD9A was down-regulated in co-exposed keratinocytes as it was also in cells subjected to UVB (Figure 13-b), but not to protons (Figure 13-a). The down-regulation of RIPK1, involved in necroptosis, and of ULK1, involved in autophagy, was detected solely in co-exposed cells, indicating that co-exposed cells are committed to these types of cell death.

a.

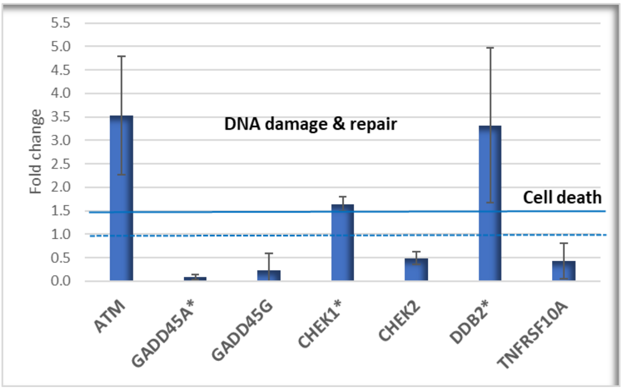

b.

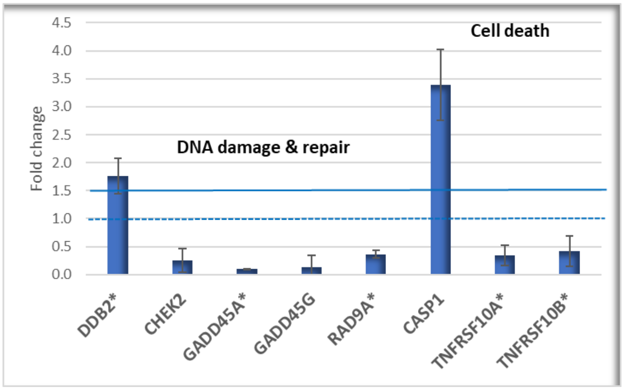

c.

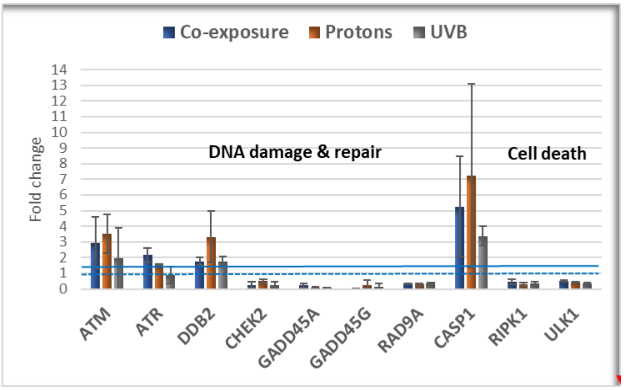

Figure 13. DNA damage and cell death genes with modified expression in human normal HaCaT keratinocytes exposed to 0.5 Gy protons or 50 J/m^2 UVB applied as single stressors, or combined (proton irradiation followed by UVB exposure within 20 min). Genes with mean fold change > 1.5 (gene up-regulation) or < 0.7 (gene down-regulation) were represented as mean value ± SD in 3 independent experiments. Genes with a significant fold change value in 2 out of 3 experiments and no significant effect in the third experiment were marked with *. The blue line is the low threshold for significant gene up-regulation, while the dashed blue line corresponds to “the no effect” case to which gene down-regulations are reported. **a**. HaCaT keratinocytes exposed to protons; **b**. HaCaT keratinocytes exposed to UVB; **c**. HaCaT keratinocytes co-exposed to protons and UVB.

[37] Miao EA, Rajan JV, Aderem A. Caspase-1-induced pyroptotic cell death. Immunol Rev. 2011 Sep;243(1):206-14. doi: 10.1111/j.1600-065X.2011.01044.x.

Besides DNA damage and cell death genes (Figure 13) several other stress genes had modified expression HaCaT keratinocytes in the investigated exposure settings (Figure 14), as presented below.

An antioxidant response was highlighted (Figure 14-a) by the over-expression of FTH1 (iron metabolism), GSTP1 (glutathionylation), and PRDX1 (reduction of hydrogen peroxide and alkyl hydroperoxides). Only FTH1 was selectively up-regulated in the co-exposure setting as compared with the exposure to protons or UVB as single stressors ($p<0.5$). The expression changes of the other antioxidant genes mentioned above were similar in all the irradiation scenarios.

a. b.

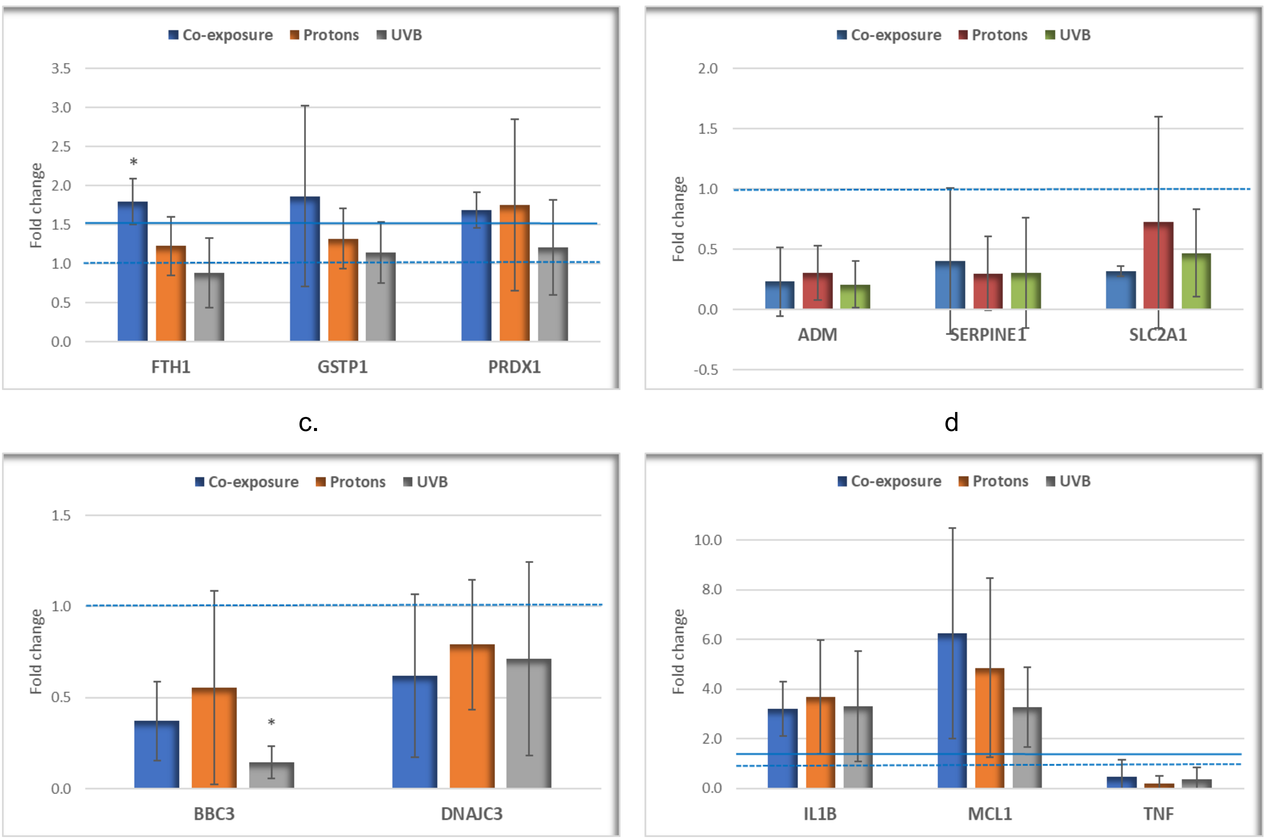

Figure 14. Stress genes with modified expression, related to antioxidant, hypoxia, and inflammatory responses, in human normal HaCaT keratinocytes exposed to 0.5 Gy protons or 50 J/m^2 UVB applied as single stressors, or combined (proton irradiation followed by UVB exposure within approx. 20 min). Genes with mean FC > 1.5, or < 0.67 were represented as mean value ± SD in 3 independent experiments. The blue line is the low threshold for significant gene up-regulation, while the dashed blue line corresponds to “the no effect” case to which gene down-regulations are reported. **a**. Antioxidant response; **b**. Hypoxia response; **c**. Unfolded protein response; **d**. Inflammation.

Several genes involved in the hypoxia response (ADM, SERPINE1 and SLC2A1) were down-regulated, while the ARNT gene was up-regulated across all the investigated settings (co-exposure: FC = 8.1 ± 9.28; protons: FC = 6.78 ± 5.19; UVB: FC = 12.03 ± 18.28), with no statistical differences between conditions (Figure 14-b). Results indicate that the hypoxia response had active components, but other associated mechanisms were profoundly down-regulated at 48 h post-exposure of HaCaT keratinocytes.

Down-regulations were registered also in the pro-apoptotic BBC3 gene[38] or DNAJC3 gene encoding the heat shock protein HSP40, part of the unfolded protein response[39] (Figure 14-c). Down-regulation was registered across all the investigated exposure types, irrespective if stressors were applied alone or in combination.

The over-expression of IL1B[40] and MCL1[41] (Figure 14-d) indicated that inflammation was active in exposed keratinocytes irrespective of the irradiation setting. The concomitant over-expression of CASP1 is indicative that the IL-1 response might be indeed fully active[42]. In turn, TNF[43] was found down-regulated (Figure 14-d), indicating a limitation in the inflammatory response.

CRL 9855 monocytes

The stress response of human normal CRL 9855 monocytes exposed to 0.5 Gy protons was characterized at 24 h after exposure by the down-regulation of multiple stress genes (Table 2). By lowering the proton dose to 0.25 Gy, only several genes were down-regulated (Table 3), while the other investigated stress genes did not have significant expression changes, indicating a dose-dependent stress response.

Most of the down-regulated stress genes in proton exposure were also found down-regulated in cells exposed to 50 J/m^2 UVB applied as a single stressor, and in cells co-exposed to protons and UVB (Table 2). There was only one notable exception: the TNFRSF1 gene[44] involved in necrotic cell death, which was down-regulated only in monocytes co-exposed to protons and UVB, while single stressors did not significantly affect their expression ($p<0.05$) (Table 2).

Table 2. The expression pattern of stress genes in CRL 9855 exposed to 0.5 Gy protons or 50 J/m2 UVB as single stressors, or co-exposed to protons and UVB. Expression changes were presented as fold change (FC) (mean value and SD for 2 independent experiments). FC values < 0.67 were considered significant for gene down-regulation.

	Protons (0.5 Gy)		**UVB (50 J/m^2)**		**Protons + UVB**	
Stress pathway/genes	Mean FC	SD	Mean FC	SD	Mean FC	SD
Cell death						
CASP1	0.18	0.03	0.16	0.01	0.18	0.05
FAS	0.19	0.03	0.26	0.10	0.31	0.17
TNFRSF1A	0.84	0.20	0.85	0.08	0.49	0.00
ATG12	0.20	0.00	0.30	0.03	0.27	0.02
ATG5	0.18	0.04	0.42	0.19	0.25	0.10
ATG7	0.29	0.12	0.79	0.08	0.22	0.03
BECN1	0.30	0.08	0.44	0.03	0.32	0.13
BNIP3L	0.24	0.02	0.29	0.04	0.27	0.08

[38] Han J, Flemington C, Houghton AB, Gu Z, Zambetti GP, Lutz RJ, Zhu L, Chittenden T. Expression of bbc3, a pro-apoptotic BH3-only gene, is regulated by diverse cell death and survival signals. Proc Natl Acad Sci U S A. 2001 Sep 25;98(20):11318-23. doi: 10.1073/pnas.201208798.
[39] Gehrmann M, Marienhagen J, Eichholtz-Wirth H, Fritz E, Ellwart J, Jäättelä M, Zilch T, Multhoff G. Dual function of membrane-bound heat shock protein 70 (Hsp70), Bag-4, and Hsp40: protection against radiation-induced effects and target structure for natural killer cells. Cell Death Differ. 2005 Jan;12(1):38-51. doi: 10.1038/sj.cdd.4401510.
[40] Liu W, Ding I, Chen K, Olschowka J, Xu J, Hu D, Morrow GR, Okunieff P. Interleukin 1beta (IL1B) signaling is a critical component of radiation-induced skin fibrosis. Radiat Res. 2006 Feb;165(2):181-91. doi: 10.1667/rr3478.1.
[41] Liang YY, Niu FY, Xu AA, Jiang LL, Liu CS, Liang HP, Huang YF, Shao XF, Mo ZW, Yuan YW. Increased MCL-1 synthesis promotes irradiation-induced nasopharyngeal carcinoma radioresistance via regulation of the ROS/AKT loop. Cell Death Dis. 2022 Feb 8;13(2):131. doi: 10.1038/s41419-022-04551-z.
[42] Sansonetti PJ, Phalipon A, Arondel J, Thirumalai K, Banerjee S, Akira S, Takeda K, Zychlinsky A. Caspase-1 activation of IL-1beta and IL-18 are essential for Shigella flexneri-induced inflammation. Immunity. 2000 May;12(5):581-90. doi: 10.1016/s1074-7613(00)80209-5.
[43] Sharma MR, Mitrani R, Werth VP. Effect of TNFα blockade on UVB-induced inflammatory cell migration and collagen loss in mice. J Photochem Photobiol B. 2020 Dec;213:112072. doi: 10.1016/j.jphotobiol.2020.112072.
[44] Lee KJ, Park KH, Hahn JH. Alleviation of Ultraviolet-B Radiation-Induced Photoaging by a TNFR Antagonistic Peptide, TNFR2-SKE. Mol Cells. 2019;42(2):151-160. doi: 10.14348/molcells.2018.0423.

DNA damage response						
ATM	0.31	0.06	0.35	0.17	0.57	0.35
ATR	0.34	0.14	0.41	0.10	0.48	0.19
Unfolded protein response						
BID	0.24	0.04	0.36	0.04	0.39	0.10
CALR	0.26	0.10	0.31	0.03	0.19	0.11
HSP90B1	0.35	0.15	0.41	0.07	0.41	0.15
HSPA4	0.38	0.16	0.38	0.05	0.40	0.13
HSPA5	0.42	0.22	0.47	0.11	0.34	0.16
Oxidative stress						
FTH1	0.37	0.19	0.35	0.00	0.43	0.09
PRDX1	0.57	0.08	0.63	0.04	0.74	0.04

Table 3. The expression changes of stress genes in CRL 9855 exposed to protons of 0.5 Gy or 0.25 Gy. Expression changes were presented as fold change (FC). FC values < 0.7 were considered significant for gene down-regulation. Results are expressed as mean value and SD. N=4 independent experiments for 0.5 Gy protons, and 2 independent experiments in the case of 0.25 Gy protons. In grey shadow are marked significant gene down-regulations in monocytes exposed to 0.25 Gy protons.

Pathway/genes	**Proton exposure**			
	0.5 Gy		**0.25 Gy**	
	Mean FC	**SD**	**Mean FC**	**SD**
Cell death				
GRB2	0.57	0.09	0.80	0.25
PVR	0.53	0.11	0.78	0.23
ATG7	0.45	0.21	0.39	0.06
BECN1	0.49	0.24	0.61	0.26
BNIP3L	0.49	0.31	0.66	0.33
DNA damage				
TP53	0.56	0.09	0.99	0.62
HUS1	0.49	0.28	0.80	0.09
MRE11A	0.59	0.28	1.00	0.01
Unfolded protein response				
ATF6	0.40	0.32	0.56	0.45
ATF6B	0.47	0.17	0.41	0.16
Antioxidant response				
GSR	0.55	0.13	0.69	0.07
Hypoxia response				
SLC2A1	0.55	0.10	0.82	0.37
VEGFA	0.64	0.32	1.04	0.06
Inflammation				
IL1A	0.45	0.31	0.78	0.07
Osmotic stress				
SLC5A3	0.51	0.10	0.95	0.57

Exposure of monocytes to UVB alone and their co-exposure to protons and UVB induced the over-expression of the inflammatory genes IL1 and IL1B, while protons alone induced the down-regulation of these genes in CRL 9855 monocytes (Figure 15). Moreover, it was found that UVB and the co-exposure of monocytes to UVB and protons did not alter the expression of the pro-inflammatory genes IL6 and CXCL8, whilst protons strongly down-regulated these genes (Figure 15).

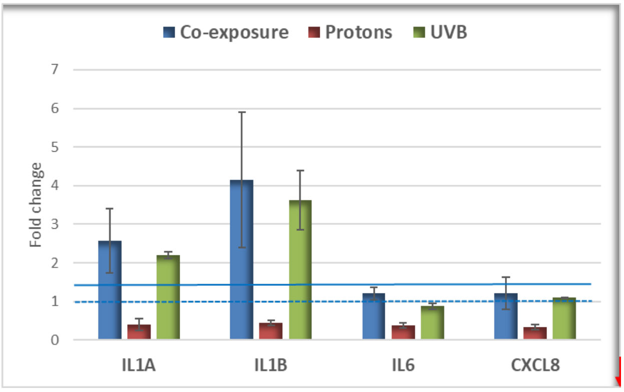

Figure 15. Inflammation genes with modified expression in human normal CRL 9855 monocytes exposed to 0.5 Gy protons or 50 J/m^2 UVB applied as single stressors, or combined (proton irradiation followed by UVB exposure within 20 min). Genes with mean FC > 1.5 (gene up-regulation) or < 0.7 (gene down-regulation) were represented as mean value ± SD in 2 independent experiments. The blue line is the low threshold for significant gene up-regulation, while the dashed blue line corresponds to "the no effect" case to which gene down-regulations are reported.

Noteworthy is that the stress response of monocytes was enhanced following fluence-effect curves when cells were exposed to UVB fluences higher than 50 J/m^2 (Figure 16). Even if some genes were not over-expressed at 50 J/m^2, they became significantly over-expressed at UVB fluences of 100 and 200 J/m^2. A tremendous increase of the FC value was registered in the case of the IL6 gene (50 J/m^2: FC = 0.75 ± 0.13; 100 J/m^2: FC = 181 ± 5; 200 J/m^2: FC = 320 ± 292 J/m^2).

a.

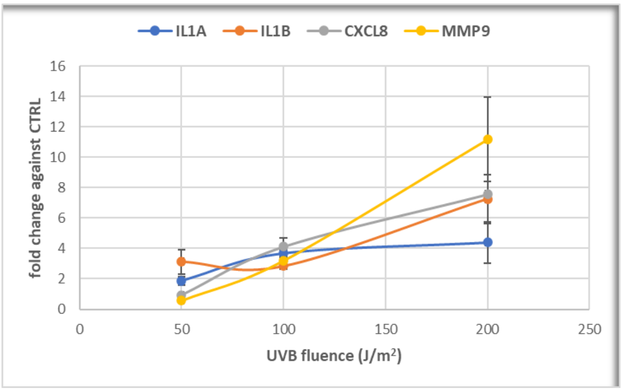

b.

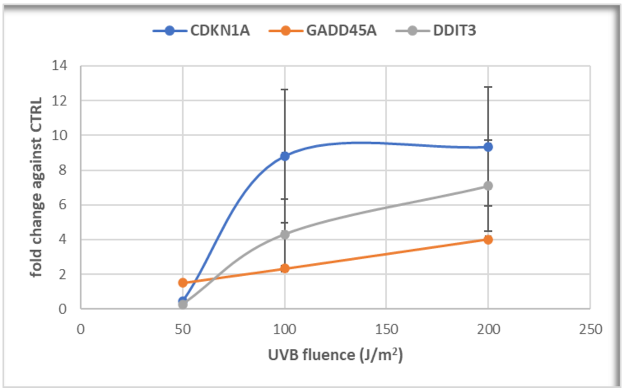

c. d.

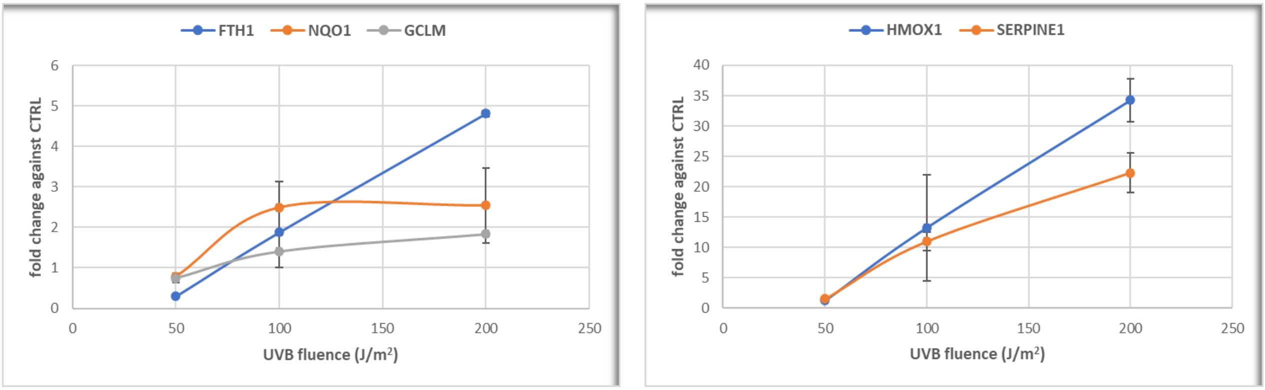

Figure 16. UVB fluence-gene expression curves for stress genes in CRL 9855 monocytes. Results are expressed as mean FC value ± SD for 2 independent experiments. **a**. Inflammation genes; **b**. DNA damage and endoplasmic reticulum stress genes; **c**, Antioxidant genes; **d**. Hypoxia genes.

Altogether, results suggest that cellular stress inflicted by the co-exposure of CRL 9855 monocytes to 0.5 Gy protons and 50 J/m^2 UVB is largely governed by UVB exposure, as seen in the viability and stress gene expression changes. A fluence increase above 50 J/m^2 was shown to elicit a strong and broad stress response.

Early versus *late stress responses*

The above-mentioned stress gene expression results characterized late stress responses in human normal cells, registered at 48 h post-exposure. A comparison was performed between these late responses at 48 h and early responses at 6 h after cell irradiation.

A higher stress response associated with DNA damage and repair Figure 17-a) was detected in co-exposed Hs27 fibroblasts at 6h post-exposure (CDKN1A, GADD45A, and DDB2). Gene overexpression decreased over time (at 48 h), indicating an ongoing cellular response to persistent DNA damage. Conversely, the XPC gene, which encodes a protein essential for Global Genome Nucleotide Excision Repair, was under-expressed at 6 h and significantly overexpressed at 48 h after cell irradiation, suggesting that some DNA repair mechanisms become active at later stages. Other genes involved in cell death (FAS) or in inflammation (IL1B) were equally expressed at 6 h and 48 h.

A different stress response was registered in HaCaT keratinocytes (Figure 17-b). The ATM gene, involved in detecting DNA double-strand breaks, was overexpressed in later stages of the DNA damage response, as well as the pro-inflammatory IL1B gene. Meanwhile, the pro-apoptotic BBC3 gene was overexpressed in early stages, its expression drastically decreasing over time, likely because damaged cells were less committed to cell death (also evident in the viability results in Figure 9). Different cells appear to cope differently with the DNA damage inflicted by the co-exposure to protons and UVB. Late stress responses are relevant for evaluating the fate of cells and potentially persistent health consequences. By comparing late and early stress responses, a therapeutic strategy might be designed for early intervention to alleviate the damage inflicted by complex radiation fields.

a)

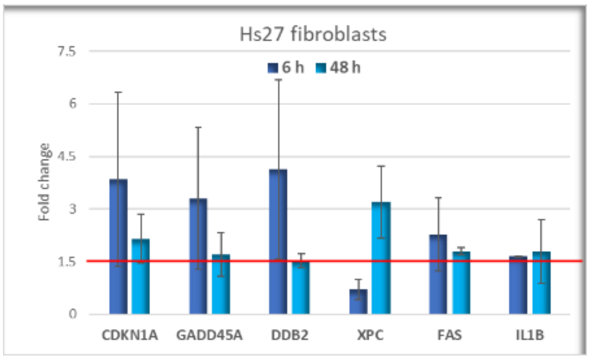

b)

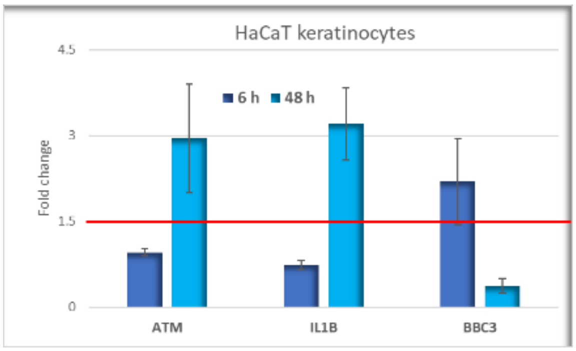

Figure 17. The dynamics of stress gene expression in human normal Hs27 fibroblasts and HaCaT keratinocytes exposed to combined radiation fields (0.5 Gy proton irradiation followed by 50 J/m^2 UVB exposure within 20 min). Genes with mean FC > 1.5 (gene up-regulation) or < 0.7 (gene down-regulation) were represented as mean value ± SD in triplicate samples. The red line is the low threshold for significant gene up-regulation. Results are presented as mean fold change (FC) value ± SEM for triplicates.

The stress response in a low-radiation background

We further investigated the stress response induced by low-level radiation background (natural radiation background in the on-ground IVB laboratory), considering as a reference the cellular response in the Unirea salt mine, in the underground IFIN “Horia Hulubei” laboratory, where a significantly lower radiation background was measured (see Materials and Methods).

Results (Figure 18) indicate that HaCaT keratinocytes cultivated on the ground overexpressed a plethora of stress genes in response to the natural radiation background, addressing DNA damage and repair, cell death (Figure 18-a), as well as inflammation, oxidative stress, and the hypoxia response (Figure 18-b). Interestingly, this tress response drastically decreased when cells were grown in a low-radiation background in the salt mine, indicating that cells can quickly adapt to various levels of environmental radiation.

Relative to the irradiation experiments with 0.5 Gy protons, results indicate that cells possess a broad range of adaptation mechanisms in response to radiation, depending on the radiation quality and dose. Nevertheless, it appears to be a threshold of the intensity of stress gene expression changes, limiting the stress response in cells exposed to intense or combined challenges.

a)	b)

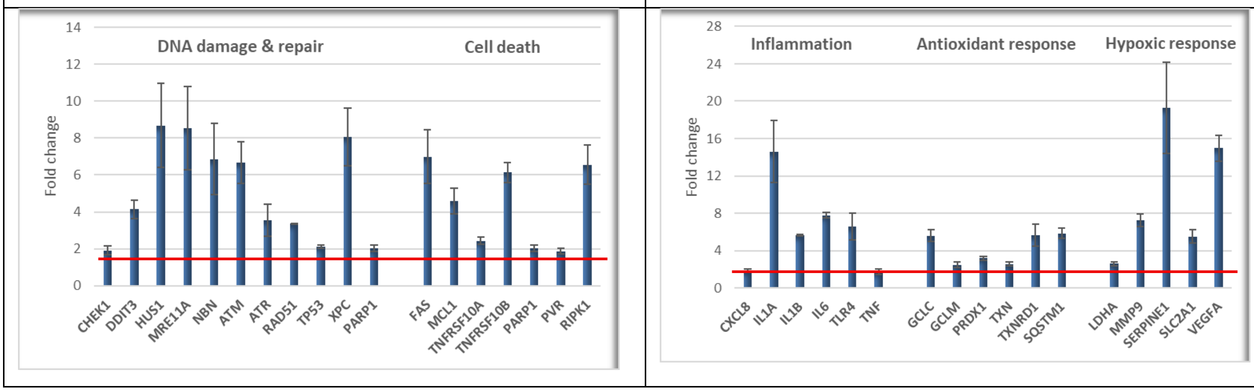

Figure 18. The expression changes of stress genes in human HaCaT keratinocytes cultivated for 72 h in the on-ground IVB laboratory, having as a reference the gene expression pattern in cells cultivated in a low-level radiation background in the underground IFIN "Horia Hulubei" laboratory, located in the Unirea salt mine (Slanic-Prahova, Romania). Only genes with an FC value > 1.5 (red line) were represented as being significantly overexpressed. Results are presented as mean fold change (FC) value ± SEM for triplicates.

DNA damage

DNA Damage and Repair was assessed by means of γH2AX immunofluorescence (IF) in fibroblasts and keratinocytes exposed to 0.5 Gy protons and UVB (100 J/m^2 and 50 J/m^2 for fibroblasts, and (50 – 25) J/m^2 for keratinocytes), either as single or combined radiations. Two experimental settings regarding the succession of the co-exposure of cells to protons and UVB were investigated: in one setting, cells were exposed to protons first and then, within approximately. 20 min, to UVB; in another setting, cells were exposed first to UVB, and then to protons. Both the number of γH2AX foci per nucleus and pan-nuclear-stained cells were analysed. Irradiated cells and controls were analysed at 1 h, 4 h, and 24 h post-exposure for fibroblasts, and 1 h, 6 h, and 24 h post-exposure for keratinocytes.

Human normal Hs27 skin fibroblasts

Irradiation of Hs27 skin fibroblasts with 0.5 Gy protons induced an increased number of γH2AX foci per nucleus at 1 h post-exposure, which declined in time, as observed at 4 h and 24 h (Figure 19-a). Meanwhile, UVB (100 J/m^2 and 50 J/m^2) increased persistently the number of γH2AX foci per nucleus, at 4 h and 24 h post-exposure (Figure 19-a). When cells were exposed to protons first and then to UVB, a synergistic effect of these radiations was observed (Figure 19-a). Thus, samples exposed to the combination of 0.5 Gy protons and 50 J/m² or 100 J/m² UVB displayed at the 1 h time point markedly higher levels of γH2AX foci per nucleus compared to cells exposed to protons or UVB alone, indicating a potential synergistic interaction between radiations in Hs27 fibroblasts.

Pan-nuclear stained Hs27 fibroblasts with γH2AX antibody were counted and the percentage was analysed (Figure 19-b). Pan-nuclear γH2AX staining mediated by ATM or DNA-PK phosphorylation it shows excessive stress due to highly repair-resistant complex damage, leading usually to apoptotic cell death[45]. Cells exposed to 0.5 Gy protons alone showed minimal pan-nuclear γH2AX staining across all time points. In contrast, UVB exposure (50 J/m² and 100 J/m²) induced a notable increase in pan-nuclear staining, particularly at 1 h and 4 h, with a decline at 24 h. Co-exposure of cells to 0.5 Gy protons, and either to 50 J/m² or 100 J/m² UVB enhanced significantly the increase of the percentage of pan-nuclear stained cells in comparison with cells exposed to single radiation, especially at 1 h (42,28% and 49,12% with 50 J/m² or 100 J/m² UVB) and 4 h (50,91% and 64,71% with 50 J/m² or 100 J/m² UVB) post-exposure. The highest percentage of pan-nuclear staining was observed in the samples co-exposed to 0.5 Gy and 100 J/m² at the 4 h time point. Results indicate a synergistic enhancement of the DNA damage response in co-exposed Hs27 fibroblasts, and that the combination of proton irradiation and UVB exposure elicited a marked increase in pan-nuclear γH2AX staining,

[45] Meyer B, Voss KO, Tobias F, Jakob B, Durante M, Taucher-Scholz G. Clustered DNA damage induces pan-nuclear H2AX phosphorylation mediated by ATM and DNA-PK. Nucleic Acids Res. 2013;41(12):6109-18. doi: 10.1093/nar/gkt304.

reflecting a broadly enhanced DNA damage and repair signalling in fibroblasts. The slower decline in γH2AX foci over time in the combined treatment group indicates that the repair mechanisms may be overwhelmed or that more complex DNA damages were induced, requiring longer repair times (resistance). These data support the hypothesis that co-exposure to protons and UVB results in higher DNA damage than either exposure alone, potentially due to the additive or synergistic effects of the two types of radiation.

In the second irradiation setting, cells were first exposed to UVB, and, within approximately. 20 min, to protons, and were analysed at 4 h and 24 h post-exposure. The number of γH2AX foci per nucleus was slightly elevated after 4 h, but significantly decreased at the 24h time point in Hs27 fibroblasts exposed to 0.5 Gy protons applied as a single radiation (Figure 20-a). Results indicate a reduction in DNA damage over time, as cells attempt to repair proton-induced double-strand breaks. Cells exposed to 100 J/m² of UVB radiation showed a similar trend, with an increase in γH2AX foci at 4 h, followed by a reduction at 24 h (Figure 20-a), suggesting a typical DNA damage response to UVB exposure[46]. In the combined exposure setting of 0.5 Gy + 100 J/m², the number of γH2AX foci per nucleus was markedly higher compared to either treatment applied alone. The average number of foci reached ~5.0 foci/nucleus at 4 h, and decreased to ~3.5 foci per nucleus at 24 h post-exposure (Figure 20-a). This significant increase in γH2AX foci suggests a synergistic effect when protons and UVB are combined, leading to enhanced DNA damage.

a. b.

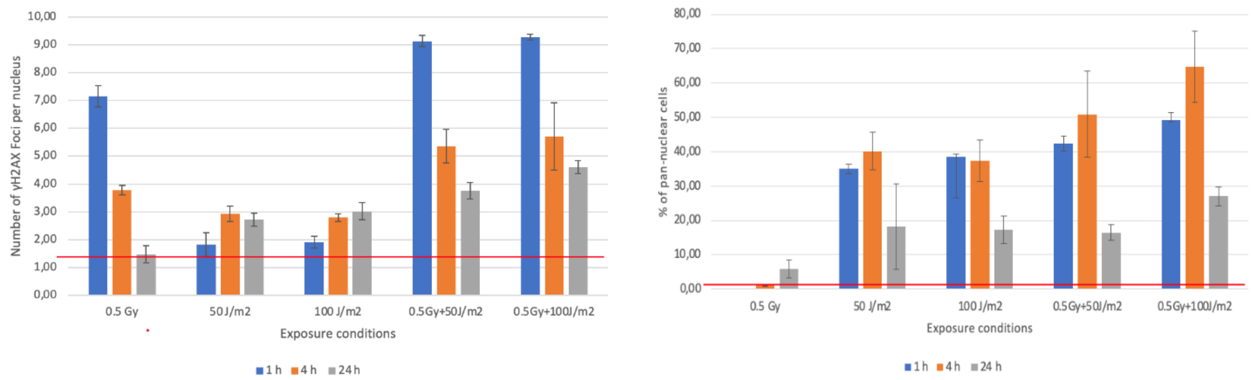

Figure 19. γH2AX staining in normal Hs27 fibroblasts at 1 h, 4 h, and 24 h after exposure to 0.5 Gy protons or UVB (50 J/m^2 or 100 J/m^2) as single stressors, or to combined challenges (protons first, and UVB approx. 20 min thereafter). Results are presented as mean number of γH2AX foci per nucleus ± SD for 2 independent experiments. The red line designates the mean value in control samples. **a**. γH2AX foci per nucleus; **b**. Pan nuclear γH2AX staining.

A very low percentage of pan-nuclear-stained cells with γH2AX antibody was detected in Hs27 fibroblasts exposed to 0.5 Gy protons at 4h and 24 h post-irradiation (Figure 20-b), suggesting minimal occurrence of global DNA damage across the nucleus. Meanwhile, 100 J/m² UVB induced a considerably higher percentage of pan-nuclear γH2AX staining (~50% at 4 h), with a slight decrease by 24 h (Figure 20-b), indicating that UVB alone causes substantial pan-nuclear DNA damage, which decreases over time due to active repair processes.

[46] https://doi.org/10.1111/j.1751-1097.2010.00744.x

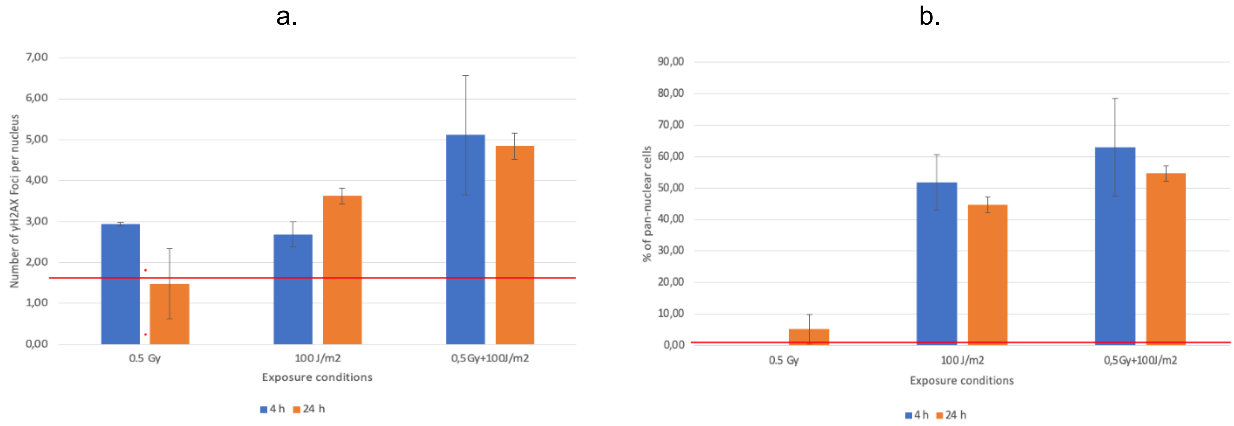

Figure 20. γH2AX staining in normal Hs27 fibroblasts at 4 h and 24 h after exposure of cells to 0.5 Gy protons or UVB (50 J/m^2 or 100 J/m^2) as single stressors, or to combined challenges (UVB first, and protons approx. 20 min thereafter). Results are presented as mean number of γH2AX foci ± SD for 2 independent experiments. The red line designates the mean value in control samples. **a**. γH2AX foci per nucleus; **b**. Pan nuclear γH2AX staining.

Comparing the two investigated exposure settings, protons followed by UVB, and UVB followed by protons, it appears that the latter setting resulted in the highest levels of pan-nuclear staining at 4 h, which slightly decreased by 24 h, remaining still significantly higher compared to the single exposures. This suggests a strong synergistic effect between protons and UVB, when UVB was applied first and protons second, leading to enhanced DNA damage across the nucleus. However, the persistence of DNA damage at 24 h post-exposure indicates that the repair mechanisms may be overwhelmed by the combination of the two radiation types. Notable differences in the DNA damage response, as measured by γH2AX foci formation in Hs27 cells, were evidenced between the two investigated irradiation settings. When cells were exposed to protons, followed by UVB exposure, the number of γH2AX foci per nucleus peaked at around 9 foci at 1 h, both for 0.5 Gy + 50 J/m² and 0.5 Gy + 100 J/m² exposures (Figure 19-a). This high initial number of foci suggests significant DNA damage from the combination of proton and UVB radiation. However, over time, there was a noticeable decrease in the number of foci, with levels dropping to around 3-4 foci per nucleus at 24 h. This decline indicates that cells were able to repair much of the damage, although a substantial amount of residual DNA damage remained. The fact that DNA repair is still ongoing at 24 h suggests that the combined damage from both radiation types may be more complex, requiring longer repair times.

When cells were exposed to UVB first, followed by protons, the trend in γH2AX foci formation was slightly different. The initial number of foci at 1 h was found again to be elevated (~8-9 foci per nucleus, Figure 20-a), like in the first scenario (Figure 19-a). However, the decline in foci over time appeared more gradual, with a larger number of residual foci persisting at the 24 h mark (around 4-5 foci per nucleus). Results suggest that, when UVB exposure precedes proton irradiation, the repair mechanisms may be less efficient in handling the combined damage, or the initial UVB-induced lesions might sensitise cells to proton-induced damage, making the repair of double-strand breaks more difficult. Comparison revealed no statistically significant differences between the two conditions at any of the investigated time points (4 h and 24 h). This indicates that, despite the observed distinct trends in DNA damage and repair, the differences in γH2AX foci between the two exposure sequences were not statistically significant, and could be attributed to experimental variability rather than a true biological effect. Therefore, the overall response to combined radiation exposure, whether protons precede UVB or *vice versa*, seems to result in comparable levels of DNA damage and repair kinetics; nevertheless, there might be a stronger effect in the second scenario. The overall response to combined radiation exposure, whether protons precede UVB or vice versa, seems to result in comparable levels of DNA damage and repair kinetics.

Human normal HaCaT keratinocytes

Irradiation of HaCaT skin keratinocytes with 0.5 Gy protons caused a substantial increase in γH2AX foci, peaking at 1 h post-exposure and gradually decreasing over 6 h and 24 h (Figure 21-a). This indicates an initial strong induction of DNA double-strand breaks (DSBs) by proton irradiation, with a subsequent repair process reducing the foci over time. When HaCaT cells were exposed to UVB (25 J/m^2 and 50 J/m^2), a moderate increase in γH2AX foci was observed, with the response more pronounced with the higher UVB dose. Meanwhile, UVB persistently increased the number of γH2AX foci per nucleus later, at 4 h and 24 h post-exposure (Figure 21-a). Notably, when cells were exposed first to protons and, within approx. 20 min, to UVB, a synergistic effect of these radiations was observed (Figure 21-a). The γH2AX foci significantly increased compared to either treatment alone, particularly when cells were co-exposed to protons and the higher UVB dose, when the number of foci per nucleus was substantially higher at the 1 h mark. This synergistic effect persisted over 6 h, and was still evident at 24 h, although the foci count decreased, reflecting ongoing DNA repair processes. These results suggest that, by combining proton irradiation with UVB, an enhanced DNA damage is produced in HaCaT cells, as evidenced by the increased γH2AX foci.

The impact of combined proton and UVB irradiation on HaCaT cells was further evaluated by measuring the percentage of pan-nuclear-stained cells using the γH2AX antibody as a marker for DNA damage (Figure 21-b). The percentage of pan-nuclear stained cells that were exposed to 0.5 Gy protons remained relatively low across all time points, suggesting a limited pan-nuclear DNA damage response to proton irradiation alone. However, exposure to UVB (25 J/m² and 50 J/m²) led to a more substantial increase in the percentage of pan-nuclear stained cells, with the effect being more pronounced at 50 J/m^2. This increase was particularly notable at 1 h post-exposure, and remained elevated at 6 h, though it began to decline by 24 h, indicating a peak in the DNA damage response followed by partial repair. Combined exposure results emphasized a marked synergistic effect. The percentage of pan-nuclear stained cells was significantly higher than in either treatment alone, particularly at 1 h and 6 h post-exposure. This synergistic response was especially obvious in cells co-exposed to 0.5 Gy and 100 J/m² at the 4 h time point, where the pan-nuclear staining remained elevated even at 24 hours, highlighting a sustained DNA damage response. These findings demonstrate that, while UVB irradiation alone can induce considerable pan-nuclear DNA damage in HaCaT cells, the addition of proton irradiation significantly amplifies this effect, leading to a more robust and persistent response.

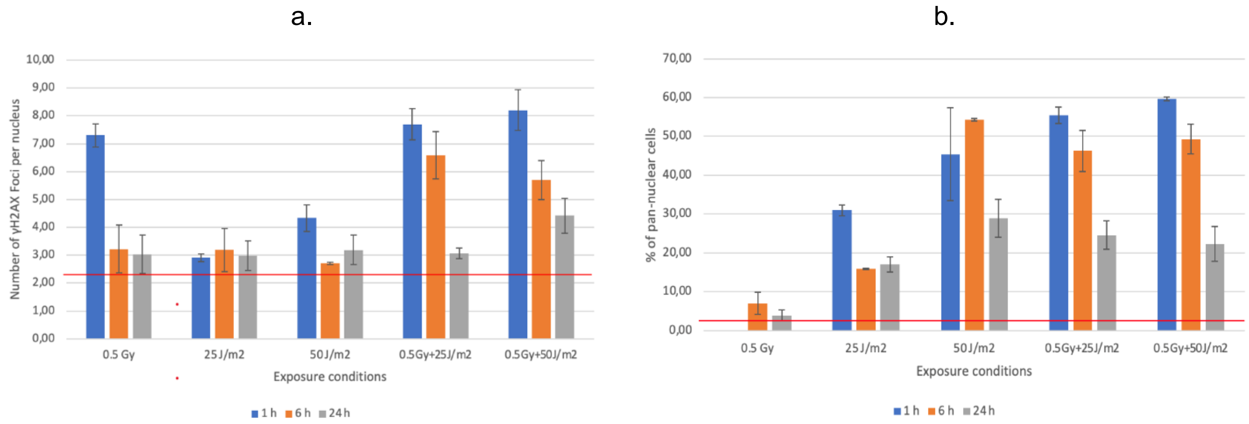

Figure 21. γH2AX staining in normal HaCaT keratinocytes at 1 h, 6 h and 24 h after exposure to 0.5 Gy protons or UVB (25 J/m^2 or 50 J/m^2) as single stressors, or to combined challenges (protons first, and UVB approx. 20 min thereafter). Results are presented as mean number of γH2AX foci per nucleus ± SD for 2 independent experiments. The red line designates the mean value in control samples. **a**. γH2AX foci per nucleus; **b**. Pan nuclear γH2AX staining.

In the second irradiation setting, cells were first exposed to UVB, and, within approximately 20 min, to protons, and were analysed at 6 h and 24 h post-exposure. A noticeable increase in γH2AX foci was observed at 6 h exposure, indicating a significant induction of DSBs, but after 24 h, the number of foci had decreased, suggesting active DNA repair mechanisms reducing the initial damage (Figure 22-a). Exposure to 50 J/m^2 of UVB alone produced a moderate increase in γH2AX foci, with a similar trend of peak foci at 6 h, followed by a reduction at 24 hours (Figure 22-a). This pattern reflects the typical DNA damage response to UVB irradiation, where damage is initially high but is progressively repaired over time. Importantly, the combined exposure setting of 0.5 Gy + 50 J/m² led to a synergistic effect with the highest number of γH2AX foci observed at 6 h (Figure 22-a). This combined exposure condition resulted in significantly more DNA damage than either treatment alone, as evidenced by the elevated γH2AX foci. Although the foci count decreased by 24 hours (Figure 22-a)., their number remained higher than the levels observed with individual exposures, indicating that the combined treatment induces more persistent DNA damage. These results underscore the synergistic interaction between UVB and proton irradiation, where the combination of both radiation types leads to enhanced and prolonged DNA damage in HaCaT cells.

The percentage of pan-nuclear stained cells remained relatively low, with a slight increase observed at 24 h. This suggests that proton irradiation induces a limited pan-nuclear DNA (Figure 22-b). Meanwhile, exposure to 50 J/m^2 of UVB alone led to a more pronounced increase in the percentage of pan-nuclear stained cells, particularly at 6 h when the damage response was at its peak. There was a noticeable reduction in pan-nuclear staining at 24 h, indicating that keratinocytes were able to initiate DNA repair processes to mitigate the UVB-induced damage (Figure 22-b). However, the most significant finding was observed when the cells were exposed to a combination of 50 J/m^2 UVB followed by 0.5 Gy of protons. This combined exposure resulted in a dramatic increase in the percentage of pan-nuclear stained cells at 6 h, much higher than the levels induced by either treatment alone. Even at 24 h, the levels remained substantially higher compared to the individual exposures, although there was a reduction in pan-nuclear staining (Figure 20-b). These results highlight the synergistic effects of combining UVB and proton irradiation, where the combination leads to significantly enhanced and sustained DNA damage compared to individual treatments. The marked increase in pan-nuclear staining following combined exposure suggests that the cells experienced a more extensive and persistent DNA damage response, likely due to the combined effects of the two types of radiation.

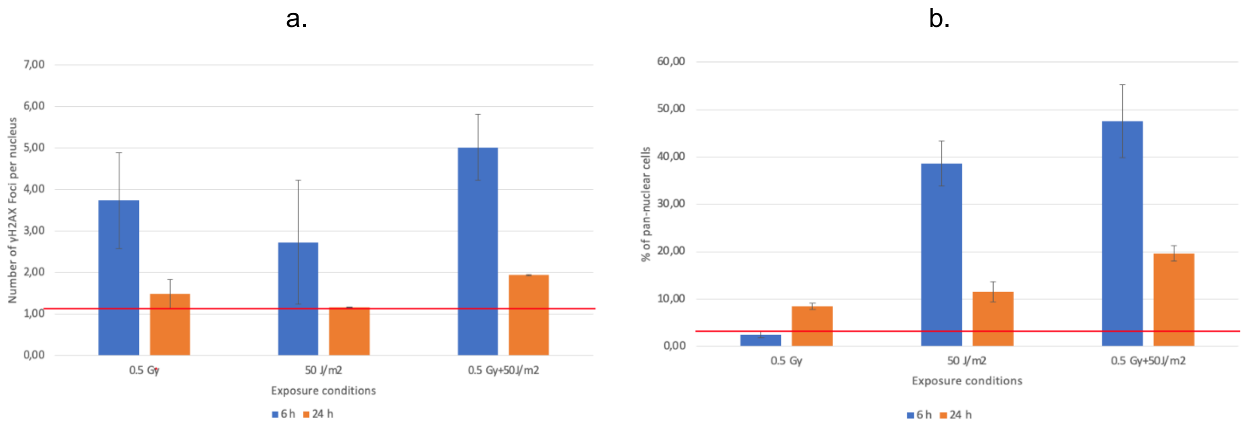

Figure 22. Mean percentage of pan-nuclear stained normal HaCaT keratinocytes with γH2AX antibody, assessed at 6 h and 24 h after exposure to UVB (25 J/m^2 or 50 J/m^2), and thereafter, within approx. 20 min, to 0.5 Gy protons. Results are presented as mean value ± SD for 2 independent experiments. The red line designates the mean of control values. **a**. γH2AX foci per nucleus; **b**. Pan nuclear γH2AX staining.

When cells were first exposed to protons followed by UVB, there was a strong and immediate increase in DNA damage, with the effects of the damage sustained over time, particularly in the case of higher UVB doses. This suggests that proton irradiation sensitizes the cells, making them more vulnerable to subsequent UVB-induced damage. Conversely, when UVB exposure was followed by protons, the initial DNA damage response to UVB was less pronounced, but the subsequent proton exposure amplified the damage, leading to a significant increase in γH2AX foci. This indicates that while UVB alone can induce DNA damage, the addition of protons exacerbates the effect, resulting in more persistent damage. In summary, the sequence of radiation exposure plays a crucial role in determining the extent and duration of DNA damage. Proton-first exposure followed by UVB resulted in more immediate and sustained damage, while UVB-first exposure followed by protons leads to an amplified damage response. The conclusions drawn from the comparison of the two exposure sequences were further validated by statistical analysis using the Student's t-test, which revealed significant differences in γH2AX foci per nucleus at all time points examined. This statistical significance underscores the robustness of the observed effects, confirming that the sequence of exposure—whether cells are first subjected to protons followed by UVB or “vice versa”— leads to distinct and measurable differences in DNA damage response.

4 Discussion

A possible scenario of human exposure to complex radiation fields coming from Space, and reaching the Earth due to the thinning of the protective ozone layer, was experimentally investigated *in vitro* using human normal skin fibroblasts and keratinocytes, as well as normal blood monocytes, as standardized human cell lines that were exposed sequentially to energetic protons (mimicking the action of muons) and UVB radiation.

Skin is one of the most affected organs by environmental radiation. Besides fibroblasts and keratinocytes, the skin contains immune cells, like macrophages, which actively participate in maintaining the homeostasis and confer protection against various types of biotic or abiotic aggression. Circulating immune cells, like monocytes, are recruited from the blood to reinforce the protection mechanisms in the injured skin[47]. While the impact of UV radiation, either UVA or UVB, on skin cells has been extensively investigated[48], the potential interference of SCR and solar emissions with the biological effects of UVB is largely unknown. This extreme scenario is becoming more and more realistic under the threat of progressive depletion of the stratospheric ozone layer[49], demanding immediate action for generating informed science-based medical decisions to protect against or to counteract the deleterious effects of combined exposure to SCR and UVB. In our *in vitro* study, a systems medicine approach[50] was applied in the present *in vitro* study by investigating various types of skin cells. Once a basic knowledge is gained by investigating cell lines, the next step is to examine in a future project, the effects of combined proton and UVB fields on complex skin substitutes from either skin grafts or lab-made tissue[51], or at least to analyse the crosstalk between these cells.

The selected doses of protons and UVB used in this study did not have important effects on the viability of fibroblasts and keratinocytes. While proton irradiation had only minor effects, UVB decreased more the number of metabolically active cells in the investigated fluence domain. Of note is that the most sensitive cells to UVB were monocytes, followed by keratinocytes, the least sensitive cells being fibroblasts. Meanwhile, the co-exposure of normal cells to protons and UVB generally had a synergistic effect, with protons intensifying the biological effect of UVB in fibroblasts, whilst the cytotoxic effects of UVB were dominant in keratinocytes and monocytes.

The synergistic action of protons and UVB was best evidenced by the significantly enhanced DNA damages inflicted to normal skin and blood cell lines, accounting for the decreased viability of co-exposed cells. At 24 h post-exposure, less DNA damage was registered, indicating the beneficial action of repair mechanisms/ Nevertheless, residual DNA damage persisted, indicating that cells are affected in the long run, even if they are exposed to relatively low radiation doses. Moreover, results showed that cells exposed first to UVB and, 20 min thereafter, to proton beams were affected more than cells exposed first to protons and then to UVB in terms of DNA damage. While proton-first exposure followed by UVB resulted in more immediate and sustained damage, UVB-first exposure followed by protons led to an amplified damage response. For the moment, simultaneous exposure of cells to protons and UVB was not technically feasible, but is a goal of a future study.

The enhanced harmful effects of the co-exposure of cells to protons and UVB were further demonstrated by a transcriptomic study on 84 stress genes. A more complex stress response was developed by co-exposed cells, as compared to cells exposed to single radiation. Results evidenced the overexpression of stress genes involved in the DNA damage response, cell death, oxidative and hypoxic stress at 24-48 h after the co-exposure of cells. Moreover, several inflammatory genes were found upregulated in co-exposed immune and non-immune cells. Inflammation is a powerful repair mechanism in the skin, but it may lead to disease if it becomes chronic [52], as prolonged low-grade systemic inflammation has been associated with various chronic pathologies, generally preceding the overt symptoms of disease[53]. Altogether, a prolonged and complex stress response was evidenced by the transcriptomic study.

As we investigated the expression pattern of stress genes in adhered fibroblasts and keratinocytes, presumably living cells, the observed over-expression of death genes indicated that cells were committed to increased cell death, especially in the co-exposure scenario of fibroblasts. Apparently, the stress response developed by co-exposed cells was unable to repair the damage inflicted by combined proton and UVB

---

[47] Cioce A, Cavani A, Cattani C, Scopelliti F. Role of the Skin Immune System in Wound Healing. Cells. 2024;13(7):624. doi: 10.3390/cells13070624.
[48] Tang X, Yang T, Yu D, Xiong H, Zhang S. Current insights and future perspectives of ultraviolet radiation (UV) exposure: Friends and foes to the skin and beyond the skin. Environ Int. 2024;185:108535. doi: 10.1016/j.envint.2024.108535.
[49] https://www.eea.europa.eu/en/topics/in-depth/climate-change-mitigation-reducing-emissions/current-state-of-the-ozone-layer
[50] Loscalzo J, Barabasi AL. Systems biology and the future of medicine. Wiley Interdiscip Rev Syst Biol Med. 2011;3(6):619-27. doi: 10.1002/wsbm.144.
[51] Vecin NM, Kirsner RS. Skin substitutes as treatment for chronic wounds: current and future directions. Front Med (Lausanne). 2023;10:1154567. doi: 10.3389/fmed.2023.1154567.
[52] Wang Z, Qi F, Luo H, Xu G, Wang D. Inflammatory Microenvironment of Skin Wounds. Front Immunol. 2022;13:789274. doi: 10.3389/fimmu.2022.789274.
[53] Orlando FA, Mainous AG 3rd. Editorial: Inflammation and chronic disease. Front Med (Lausanne). 2024;11:1434533. doi: 10.3389/fmed.2024.1434533.

radiation, and cells may further die after the time point at which we assessed the expression changes of stress genes (24 h for monocytes and 48 h for fibroblasts and keratinocytes).

Partial fingerprints of protons and UVB effects, as well as additional stress genes with expression changes, were evidenced in co-exposed cells, indicating that co-exposed fibroblasts and keratinocytes were indeed more stressed than cells exposed either to protons or to UVB. Meanwhile, the gene expression pattern in co-exposed monocytes highlighted that these cells were sensitive to UVB, their behaviour being ruled by the effects inflicted by UVB, as was also shown by the decrease in viability. The expression of several stress genes followed a dose-effect relationship in monocytes, indicating that their stress response was even stronger at higher UVB fluences of 100-200 J/m^2. These results explained and validated the gene expression pattern registered by us in monocytes, in which many stress genes were not affected or were found down-regulated at 50 J/m^2 UVB, but became over-expressed at higher fluences. Gene down-regulation late after challenging cells with radiation might be a mechanism to resolve the stress response, probably because the inflicted damages were partially repaired. Higher UVB fluences inflicted more cellular damage, and cells developed a broader, stronger, and more persistent stress response to DNA damage, proteotoxicity, oxidative, and hypoxic stress.

We observed that the magnitude of the expression change of an individual stress gene in co-exposed cells was generally the same as in cells exposed to single radiation, suggesting that the intensity of the stress response could not increase over a certain threshold. This behaviour may account for the increased DNA lesions registered in co-exposed cells, the stress response being unable to fully repair the damage inflicted by the combined radiation fields.

Noteworthy is that we investigated relatively late cellular effects of protons and UVB at 48 h post-exposure in the case of adherent cells (fibroblasts and keratinocytes), and, at 24 h, for non-adherent monocytes. By comparing early and late stress responses, two waves of stress response were evidenced, one appearing in early stages and declining over time, and a second one being activated later due to persistent radiation-induced damage. As certain stress genes, especially in monocytes, were found down-regulated at 24 h post-exposure, it appears that the stress response was partly on its way to extinguish. Meanwhile, the registered gene up-regulation at 24 - 48 h post-exposure indicates that normal cells remain under stress late after exposure, although the investigated proton doses and UVB fluences were relatively low (0.5 Gy and 50 J/m^2, respectively). In the real world, if cells are chronically co-exposed to SCR and UVB, more damaging health effects are expected in the long run than those inflicted by solitary radiation hits[54,55]. The study that we performed in a low-radiation background indicated that cells developed a broad stress response to the normal radiation background, which was reversible when cells were moved to a very low-radiation background.

Intensive research efforts are needed to identify gene targets to reinforce and/or to prolong the repair stress response. The present study identified a panel of stress genes, common or specific for each of the investigated cell lines, that may be therapeutically targeted for alleviating the damage inflicted by the body's exposure to low-dose, combined radiation fields. The observed synergism between proton and UVB irradiation underscores the potential for increased biological impact when these types of radiation are combined, which may have important implications for understanding radiation exposure risks and the development of therapeutic strategies that leverage this enhanced response.

Based on the expression of stress genes found up-regulated in the present study, we built a stress model using the STRNG software[56] gene networks and the biological process (Gene Ontology) enrichment map for keratinocytes (Figures 23-a and 23-b) and fibroblasts (Figures 23-c and 23-d), which were co-exposed to protons and UVB. Because only the related IL1A and IL1B inflammatory genes were found consistently upregulated in monocytes at 24 h after co-exposure to protons and UVB, we built the network of genes that functionally relate to IL1A/B (Figure 24). STRING analysis evidenced the connections between the components of the stress response that were still active at 48 h in keratinocytes and fibroblasts, and at 24 h in monocytes, but did not manage to fully repair the damages inflicted by radiation, as demonstrated by the persistent DNA damage and the decrease of cellular viability. These connections emphasize that a broader

[54] Talapko J, Talapko D, Katalinić D, Kotris I, Erić I, Belić D, Vasilj Mihaljević M, Vasilj A, Erić S, Flam J, Bekić S, Matić S, Škrlec I. Health Effects of Ionizing Radiation on the Human Body. Medicina (Kaunas). 2024;60(4):653. doi: 10.3390/medicina60040653.
[55] Shin E, Lee S, Kang H, Kim J, Kim K, Youn H, Jin YW, Seo S, Youn B. Organ-Specific Effects of Low Dose Radiation Exposure: A Comprehensive Review. Front Genet. 2020;11:566244. doi: 10.3389/fgene.2020.566244.
[56] https://string-db.org

stress response might be boosted by therapeutically targeting one element of the network, but care should be taken to control the general therapy impact to avoid unwanted off-target effects.

5 Conclusion

A prolonged stress was evidenced in human normal keratinocytes, fibroblasts, and monocytes exposed *in vitro* to combined proton and UVB radiation as a mimic of increased exposure of humans to combined radiation fields reaching the Earth due to the progressive depletion of the stratospheric ozone layer. Co-exposure of cells inflicted more profound and persistent DNA damage than either radiation alone, resulting in enhanced reduction of the number of metabolically active cells and increased DNA damage. Various repair mechanisms related to DDR, inflammation, antioxidant, and hypoxia responses were identified. Gene targets, common or specific to each cell line, were identified for further shaping a therapeutic strategy aimed at alleviating the harmful effects of combined radiation exposure.

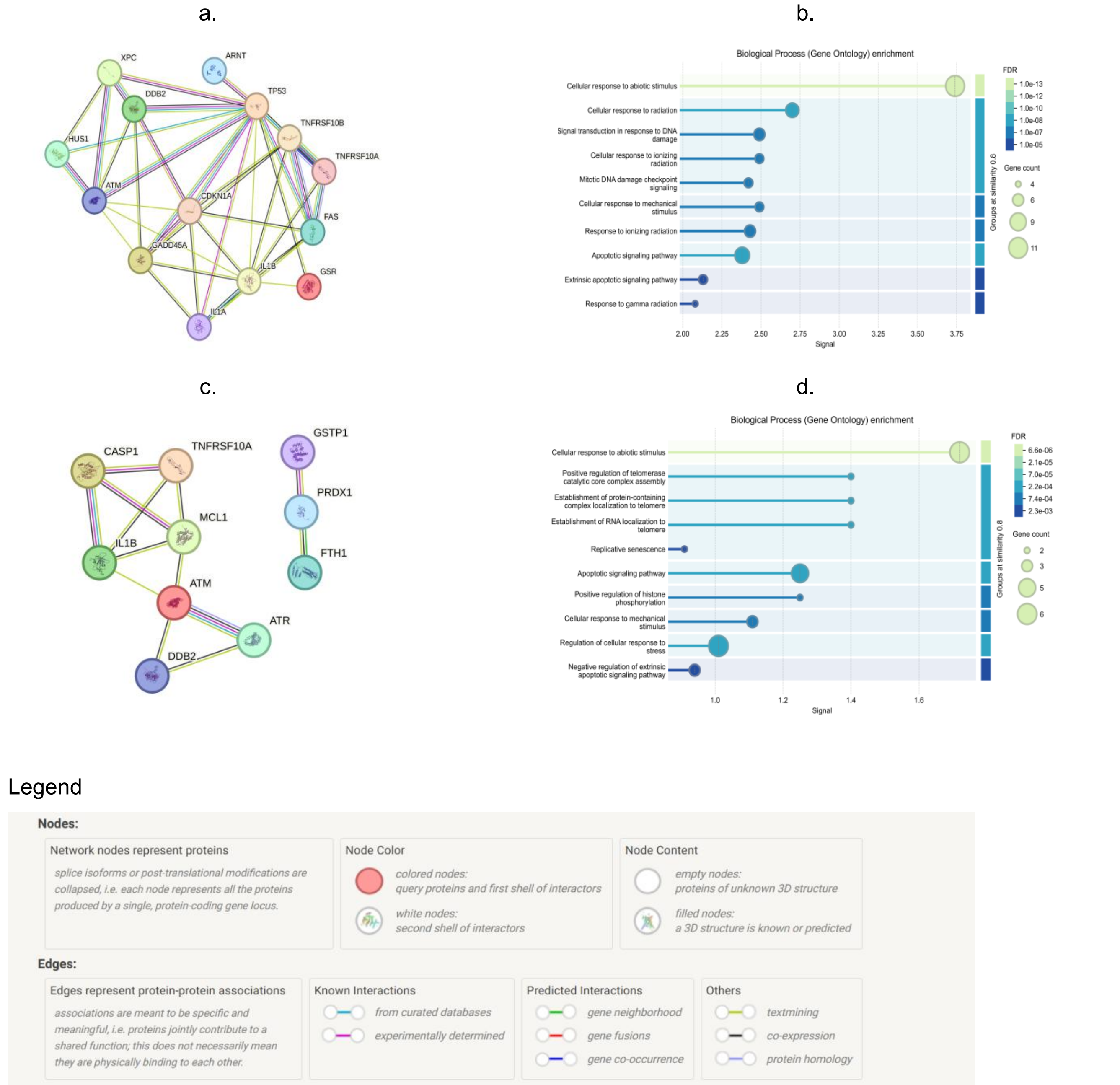

Figure 23. The network of stress genes found up-regulated in adhered human skin cell lines, and the biologic process (Gene Ontology) enrichment at 48 h after co-exposure of cells to 0.5 Gy protons, and, within 20 min, to 50 J/m^2 UVB. The analysis was performed with the STRING software for functional protein association networks (https://string-db.org/). The edges in networks indicate both functional and physical protein associations. The active interaction sources were text mining, experiments, datasets, co-expression, co-occurrence, and neighbourhood. The medium confidence coefficient of interactions was set at 0.4. **a.** the network of stress genes in Hs27 fibroblasts; **b.** the biology process in Hs27 fibroblasts; **c.** the network of stress genes in HaCaT keratinocytes; **d.** the biology process in HaCaT keratinocytes. Details on STRING analysis are presented in the Supplemental file.

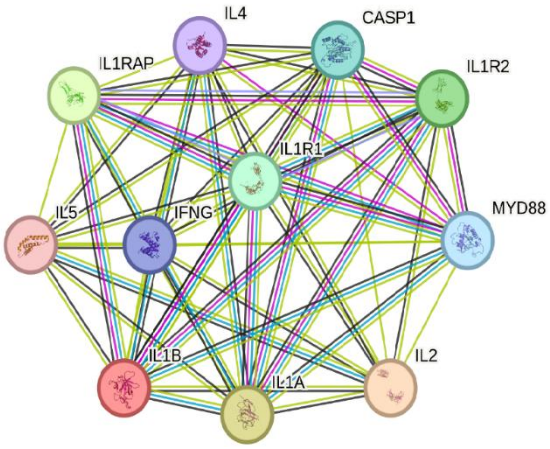

Figure 24. The network of genes related to the proinflammatory IL1A and IL1B genes that were.found up-regulated in human CRL 9855 monocytes at 24 h after co-exposure to 0.5 Gy protons, and, within 20 min, to 50 J/m^2 UVB. The analysis was performed with the STRING software for functional protein association networks (https://string-db.org/). The edges in networks indicate both functional and physical protein associations. The active interaction sources were: text mining, experiments, datasets, co-expression, co-occurrence, and neighbourhood. The medium confidence coefficient of interactions was set at 0.4

Legend

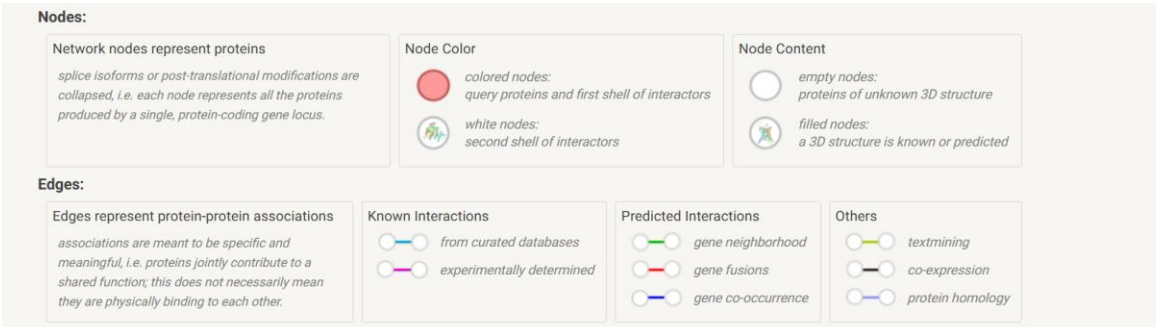

.

6 Supplemental file

STRING: functional proteins analysis

The connection between the identified stress genes that were overexpressed in human normal skin cells (Hs27 fibroblasts, and HaCaT keratinocytes), and in human normal CRL9855 monocytes was established using the STRING software (47).
The parameters used for the STRING analysis are presented in the figure below.

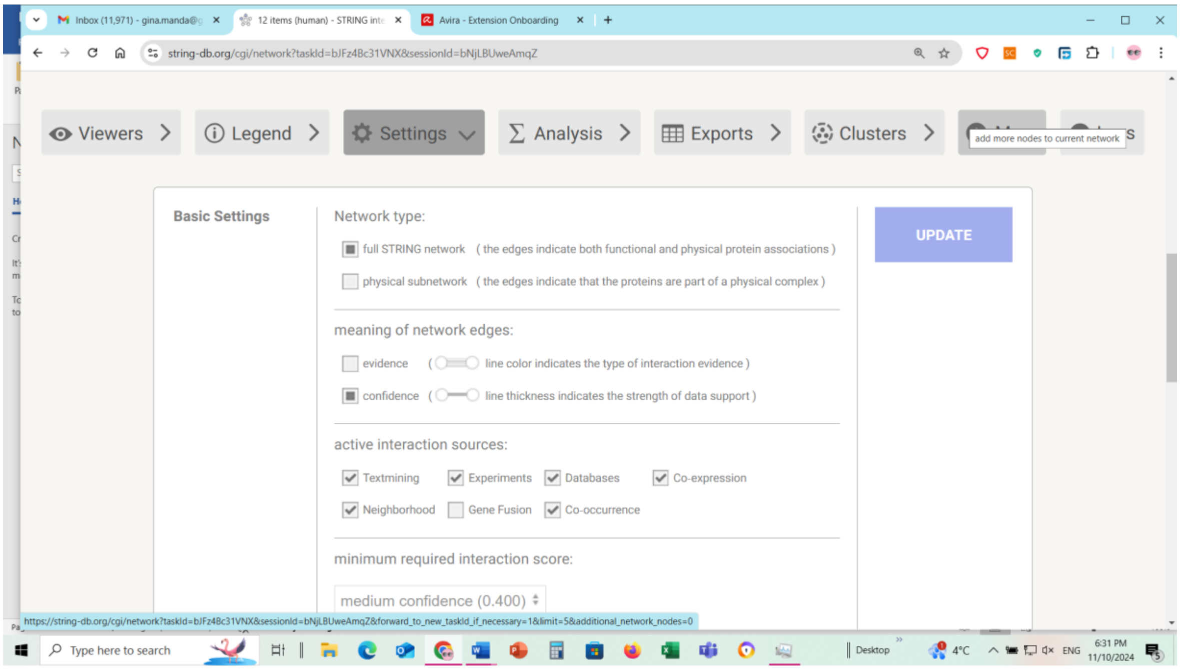

GO (Gene Ontology) enrichment analysis: FDR (false discovery rate) < 0.05.

1. FIBROBLASTS

Input

GSR	*Glutathione reductase, mitochondrial; Maintains high levels of reduced glutathione in the cytosol. (522 aa)*
TP53	*Cellular tumor antigen p53; Acts as a tumor suppressor in many tumor types; induces growth arrest or apoptosis depending on the physiological circumstances and cell type. Involved in cell cycle regulation as a trans-activator that acts to negatively regulate cell division by controlling a set of genes required for this process. One of the activated genes is an inhibitor of cyclin-dependent kinases. Apoptosis induction seems to be mediated either by stimulation of BAX and FAS antigen expression, or by repression of Bcl-2 expression. Its pro-apoptotic activity is activated via its intera [...] (393 aa)*
GADD45A	*Growth arrest and DNA damage-inducible protein GADD45 alpha; In T-cells, functions as a regulator of p38 MAPKs by inhibiting p88 phosphorylation and activity (By similarity). Might affect PCNA interaction with some CDK (cell division protein kinase) complexes; stimulates DNA excision repair in vitro and inhibits entry of cells into S phase; Belongs to the GADD45 family. (165 aa)*
XPC	*DNA repair protein complementing XP-C cells; Involved in global genome nucleotide excision repair (GG-NER) by acting as damage sensing and DNA-binding factor component of the XPC complex. Has only a low DNA repair activity by itself which is stimulated by RAD23B and RAD23A. Has a preference to bind DNA containing a short single-stranded segment but not to damaged oligonucleotides. This feature is proposed to be related to a dynamic sensor function: XPC can rapidly screen duplex DNA for non-hydrogen- bonded bases by forming a transient nucleoprotein intermediate complex which matures in [...] (940 aa)*
DDB2	*DNA damage-binding protein 2; Required for DNA repair. Binds to DDB1 to form the UV-damaged DNA-binding protein complex (the UV-DDB complex). The UV-DDB complex may recognize UV-induced DNA damage and recruit proteins of the nucleotide excision repair pathway (the NER pathway) to initiate DNA repair. The UV-DDB complex preferentially binds to cyclobutane pyrimidine dimers (CPD), 6-4*

	photoproducts (6-4 PP), apurinic sites and short mismatches. Also appears to function as the substrate recognition module for the DCX (DDB1-CUL4-X-box) E3 ubiquitin-protein ligase complex DDB1-CUL4-ROC1 (al [...] (427 aa)
HUS1	*Checkpoint protein HUS1; Component of the 9-1-1 cell-cycle checkpoint response complex that plays a major role in DNA repair. The 9-1-1 complex is recruited to DNA lesion upon damage by the RAD17-replication factor C (RFC) clamp loader complex. Acts then as a sliding clamp platform on DNA for several proteins involved in long-patch base excision repair (LP-BER). The 9-1-1 complex stimulates DNA polymerase beta (POLB) activity by increasing its affinity for the 3'-OH end of the primer-template and stabilizes POLB to those sites where LP-BER proceeds; endonuclease FEN1 cleavage activity [...] (280 aa)*
FAS	*Tumor necrosis factor receptor superfamily member 6; Receptor for TNFSF6/FASLG. The adapter molecule FADD recruits caspase-8 to the activated receptor. The resulting death-inducing signaling complex (DISC) performs caspase-8 proteolytic activation which initiates the subsequent cascade of caspases (aspartate-specific cysteine proteases) mediating apoptosis. FAS-mediated apoptosis may have a role in the induction of peripheral tolerance, in the antigen- stimulated suicide of mature T-cells, or both. The secreted isoforms 2 to 6 block apoptosis (in vitro). (335 aa)*
ARNT	*Aryl hydrocarbon receptor nuclear translocator; Required for activity of the Ah (dioxin) receptor. This protein is required for the ligand-binding subunit to translocate from the cytosol to the nucleus after ligand binding. The complex then initiates transcription of genes involved in the activation of PAH procarcinogens. The heterodimer binds to core DNA sequence 5'-TACGTG-3' within the hypoxia response element (HRE) of target gene promoters and functions as a transcriptional regulator of the adaptive response to hypoxia (By similarity). The heterodimer ARNT:AHR binds to core DNA sequ [...] (789 aa)*
ATM	*Serine-protein kinase ATM; Serine/threonine protein kinase which activates checkpoint signaling upon double strand breaks (DSBs), apoptosis and genotoxic stresses such as ionizing ultraviolet A light (UVA), thereby acting as a DNA damage sensor. Recognizes the substrate consensus sequence [ST]- Q. Phosphorylates 'Ser-139' of histone variant H2AX at double strand breaks (DSBs), thereby regulating DNA damage response mechanism. Also plays a role in pre-B cell allelic exclusion, a process leading to expression of a single immunoglobulin heavy chain allele to enforce clonality and monospec [...] (3056 aa)*
IL1A	*Interleukin-1 alpha; Produced by activated macrophages, IL-1 stimulates thymocyte proliferation by inducing IL-2 release, B-cell maturation and proliferation, and fibroblast growth factor activity. IL-1 proteins are involved in the inflammatory response, being identified as endogenous pyrogens, and are reported to stimulate the release of prostaglandin and collagenase from synovial cells. (271 aa)*
TNFRSF10A	*Tumor necrosis factor receptor superfamily member 10A; Receptor for the cytotoxic ligand TNFSF10/TRAIL. The adapter molecule FADD recruits caspase-8 to the activated receptor. The resulting death-inducing signaling complex (DISC) performs caspase-8 proteolytic activation which initiates the subsequent cascade of caspases (aspartate-specific cysteine proteases) mediating apoptosis. Promotes the activation of NF-kappa-B. (468 aa)*
CDKN1A	*Cyclin-dependent kinase inhibitor 1; May be involved in p53/TP53 mediated inhibition of cellular proliferation in response to DNA damage. Binds to and inhibits cyclin-dependent kinase activity, preventing phosphorylation of critical cyclin-dependent kinase substrates and blocking cell cycle progression. Functions in the nuclear localization and assembly of cyclin D-CDK4 complex and promotes its kinase activity towards RB1. At higher stoichiometric ratios, inhibits the kinase activity of the cyclin D-CDK4 complex. Inhibits DNA synthesis by DNA polymerase delta by competing with POLD3 [...] (164 aa)*

TNFRSF10B	*Tumor necrosis factor receptor superfamily member 10B; Receptor for the cytotoxic ligand TNFSF10/TRAIL. The adapter molecule FADD recruits caspase-8 to the activated receptor. The resulting death-inducing signaling complex (DISC) performs caspase-8 proteolytic activation which initiates the subsequent cascade of caspases (aspartate-specific cysteine proteases) mediating apoptosis. Promotes the activation of NF-kappa-B. Essential for ER stress-induced apoptosis. (440 aa)*
IL1B	*Interleukin-1 beta; Potent proinflammatory cytokine. Initially discovered as the major endogenous pyrogen, induces prostaglandin synthesis, neutrophil influx and activation, T-cell activation and cytokine production, B- cell activation and antibody production, and fibroblast proliferation and collagen production. Promotes Th17 differentiation of T-cells. Synergizes with IL12/interleukin-12 to induce IFNG synthesis from T- helper 1 (Th1) cells. (269 aa)*

Organism: Homo sapiens, *NCBI taxonomy Id: 9606*

Network

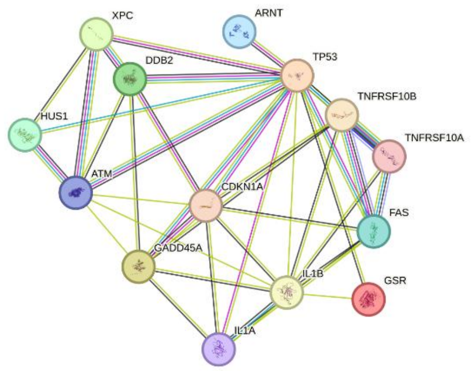

Network Stats

- number of nodes: 14
- number of edges: 40
- average node degree: 5.71
- avg. local clustering coefficient: 0.789
- expected number of edges: 12
- PPI enrichment p-value: 9.9e-11

Biologic processes (Gene Ontology)

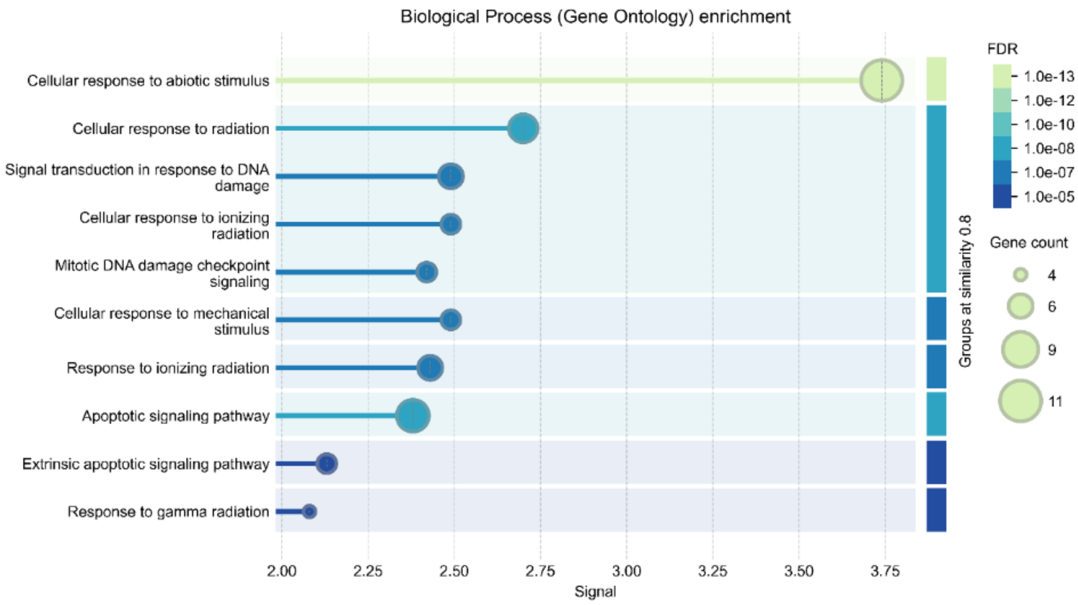

GO-term
description
count in network

strength
signal
false discovery rate

GO:0071214
Cellular response to abiotic stimulus
11 of 325

1.68
3.74
1.63e-13

GO:0071478
Cellular response to radiation
7 of 183

1.73
2.7
5.86e-08

GO:0042770
Signal transduction in response to DNA damage
6 of 135

1.8
2.49
6.76e-07

GO:0071479
Cellular response to ionizing radiation
5 of 75

1.97
2.49
2.28e-06

GO:0071260
Cellular response to mechanical stimulus
5 of 75

1.97
2.49

2.28e-06

Molecular Function (Gene Ontology)

GO-term
description
count in network
strength
signal
false discovery rate

GO:0005035
Death receptor activity
3 of 13
2.51
1.56
0.00078

GO:0045569
TRAIL binding
2 of 5
2.75
0.83
0.0242

Cellular Component (Gene Ontology)

GO-term
description
count in network
strength
signal
false discovery rate

GO:0090734
Site of DNA damage
4 of 102
1.74
1.26
0.0016

Reference Publications (PubMed)

publication
(year) title
count in network
strength
signal
false discovery rate

PMID:34371724
(2021) Insight into the Web of Stress Responses Triggered at Gene Expression Level by Porphyrin-PDT in HT29 Human Colon Carcinoma Cells.
9 of 43
2.47
6.18
2.94e-14

PMID:37415761
(2023) Modifications in cellular viability, DNA damage and stress responses inflicted in cancer cells by copper-64 ions.
8 of 45
2.4
5.02
1.16e-11

PMID:32284698

(2020) Blood Gene Expression Profile Study Revealed the Activation of Apoptosis and p53 Signaling Pathway May Be the Potential Molecular Mechanisms of Ionizing Radiation Damage and Radiation-Induced Bystander Effects.
7 of 25
2.6
4.93
5.73e-11
PMID:26997981
(2016) Genetic stability of pluripotent stem cells during anti-cancer therapies.
8 of 54
2.32
4.76
2.95e-11
PMID:32213959
(2020) Induction of p53-Dependent Apoptosis by Prostaglandin A2.
7 of 32
2.49
4.66
1.42e-10

Local Network Cluster (STRING)

cluster
description
count in network
strength
signal
false discovery rate

CL:6997
Mixed, incl. P53 DNA-binding domain, and SWIB/MDM2 domain
2 of 10
2.45
0.69
0.0449
CL:16943
TRAIL signaling
2 of 6
2.67
0.69
0.0449
CL:16155
Interleukin-1 conserved site, and Interleukin-1 receptor type 1
2 of 5
2.75
0.69
0.0449
CL:6897
Mixed, incl. G1 Phase, and G0 and Early G1
3 of 67
1.8
0.66
0.0449
CL:6148
Diseases of DNA repair, and DNA repair complex
3 of 76
1.74
0.65
0.0449

KEGG Pathways
pathway
description
count in network
strength
signal
false discovery rate
hsa04115
p53 signaling pathway
8 of 72
2.19
5.53
5.08e-14
hsa04210
Apoptosis
6 of 131
1.81
2.85
4.86e-08
hsa05216
Thyroid cancer
4 of 37
2.18
2.73
1.33e-06
hsa04218
Cellular senescence
6 of 150
1.75
2.71
7.12e-08
hsa05213
Endometrial cancer
4 of 58
1.99
2.39
4.46e-06

Reactome Pathways
pathway
description
count in network
strength
signal
false discovery rate
HSA-5218859
Regulated Necrosis
6 of 58
2.16
3.77
3.09e-09
HSA-6803211
TP53 Regulates Transcription of Death Receptors and Ligands
4 of 12
2.67
3.48
9.40e-08
HSA-5633008

TP53 Regulates Transcription of Cell Death Genes
5 of 43
2.21
3.32
5.84e-08
HSA-3700989
Transcriptional Regulation by TP53
10 of 361
1.59
3.14
1.06e-11
HSA-69416
Dimerization of procaspase-8
3 of 11
2.58
2.29
2.62e-05

WikiPathways

pathway
description
count in network
strength
signal
false discovery rate

WP707
DNA damage response
7 of 69
2.15
4.52
2.50e-11
WP1530
miRNA regulation of DNA damage response
7 of 71
2.14
4.5
2.50e-11
WP4963
p53 transcriptional gene network
6 of 90
1.97
3.34
8.62e-09
WP1742
TP53 network
4 of 19
2.47
3.19
2.73e-07
WP3982
miRNA regulation of p53 pathway in prostate cancer
4 of 24
2.37
3.02
5.04e-07

Disease-gene Associations (DISEASES)

disease
description

count in network
strength
signal
false discovery rate

DOID:11054
Urinary bladder cancer
3 of 38
2.05
0.92
0.0137

DOID:6543
Acne
2 of 4
2.85
0.92
0.0161

DOID:12704
Ataxia telangiectasia
2 of 5
2.75
0.92
0.0161

DOID:345
Uterine disease
3 of 72
1.77
0.85
0.0161

DOID:0060032
Autoimmune disease of musculoskeletal system
4 of 200
1.45
0.78
0.0161

Tissue Expression

tissue
description
count in network
strength
signal
false discovery rate

BTO:0001938
U2-OS cell
2 of 5
2.75
1.01
0.0108

BTO:0000180
Cervical carcinoma cell
5 of 322
1.34
0.91
0.0052

BTO:0003861
Inflammatory cell
2 of 14
2.3

0.81
0.0247
BTO:0002245
Foreskin fibroblast cell line
2 of 13
2.34
0.81
0.0247
BTO:0001340
Bronchus
2 of 25
2.05
0.8
0.0247

Subcellular Localization (COMPARTMENTS)

compartment
description
count in network
strength
signal
false discovery rate
GOCC:0031264
Death-inducing signaling complex
3 of 12
2.55
1.77
0.00030
GOCC:0071159
NF-kappaB complex
3 of 26
2.21
1.52
0.00079
GOCC:0031266
TRAIL death-inducing signaling complex
2 of 3
2.97
1.32
0.0027
GOCC:1990391
DNA repair complex
3 of 53
1.9
1.16
0.0036
GOCC:0045323
interleukin-1 receptor complex
2 of 7
2.6
1.12
0.0064

Human Phenotype (Monarch)

phenotype
description
count in network
strength
signal

false discovery rate
HP:0012189
Hodgkin lymphoma
3 of 20
2.32
1.25
0.0031
HP:0000524
Conjunctival telangiectasia
3 of 21
2.3
1.25
0.0031
HP:0008069
Neoplasm of the skin
5 of 175
1.6
1.23
0.0014
HP:0012539
Non-Hodgkin lymphoma
3 of 29
2.16
1.22
0.0034
HP:0100012
Neoplasm of the eye
3 of 45
1.97
1.03
0.0074

Annotated Keywords (UniProt)

keyword
description
count in network
strength
signal
false discovery rate
KW-0666
Pyrogen
2 of 2
3.15
1.4
0.0019
KW-0227
DNA damage
5 of 386
1.26
0.99
0.0019

Protein Domains (Pfam)

domain
description
count in network
strength
signal

false discovery rate
PF02394
Interleukin-1 propeptide
2 of 2
3.15
1.13
0.0065

Protein Domains and Features (InterPro)

domain
description
count in network
strength
signal
false discovery rate

IPR001368
TNFR/NGFR cysteine-rich region
3 of 25
2.23
1.09
0.0066

IPR034029
Tumour necrosis factor receptor 10A/B, death domain
2 of 2
3.15
1.07
0.0085

IPR003502
Interleukin-1 propeptide
2 of 2
3.15
1.07
0.0085

IPR000488
Death domain
3 of 35
2.08
1.02
0.0085

IPR034024
Tumor necrosis factor receptor 10, N-terminal
2 of 4
2.85
1.02
0.0101

Protein Domains (SMART)

domain
description
count in network
strength
signal
false discovery rate

SM00208
Tumor necrosis factor receptor / nerve growth factor receptor repeats.
3 of 24
2.25
1.56
0.00068

SM00005
DEATH domain, found in proteins involved in cell death (apoptosis).
3 of 27
2.19
1.55
0.00068
SM00125
Interleukin-1 homologues
2 of 10
2.45
1.05

2. KERATNOCYTES

Input

ATM	*Serine-protein kinase ATM; Serine/threonine protein kinase which activates checkpoint signaling upon double strand breaks (DSBs), apoptosis and genotoxic stresses such as ionizing ultraviolet A light (UVA), thereby acting as a DNA damage sensor. Recognizes the substrate consensus sequence [ST]- Q. Phosphorylates 'Ser-139' of histone variant H2AX at double strand breaks (DSBs), thereby regulating DNA damage response mechanism. Also plays a role in pre-B cell allelic exclusion, a process leading to expression of a single immunoglobulin heavy chain allele to enforce clonality and monospec [...] (3056 aa)*
TNFRSF10A	*Tumor necrosis factor receptor superfamily member 10A; Receptor for the cytotoxic ligand TNFSF10/TRAIL. The adapter molecule FADD recruits caspase-8 to the activated receptor. The resulting death-inducing signaling complex (DISC) performs caspase-8 proteolytic activation which initiates the subsequent cascade of caspases (aspartate-specific cysteine proteases) mediating apoptosis. Promotes the activation of NF-kappa-B. (468 aa)*
CASP1	*Caspase-1 subunit p10; Thiol protease that cleaves IL-1 beta between an Asp and an Ala, releasing the mature cytokine which is involved in a variety of inflammatory processes. Important for defense against pathogens. Cleaves and activates sterol regulatory element binding proteins (SREBPs). Can also promote apoptosis. Upon inflammasome activation, during DNA virus infection but not RNA virus challenge, controls antiviral immunity through the cleavage of CGAS, rendering it inactive. In apoptotic cells, cleaves SPHK2 which is released from cells and remains enzymatically active extracell [...] (404 aa)*
MCL1	*Induced myeloid leukemia cell differentiation protein Mcl-1; Involved in the regulation of apoptosis versus cell survival, and in the maintenance of viability but not of proliferation. Mediates its effects by interactions with a number of other regulators of apoptosis. Isoform 1 inhibits apoptosis. Isoform 2 promotes apoptosis. Belongs to the Bcl-2 family. (350 aa)*
IL1B	*Interleukin-1 beta; Potent proinflammatory cytokine. Initially discovered as the major endogenous pyrogen, induces prostaglandin synthesis, neutrophil influx and activation, T-cell activation and cytokine production, B- cell activation and antibody production, and fibroblast proliferation and collagen production. Promotes Th17 differentiation of T-cells. Synergizes with IL12/interleukin-12 to induce IFNG synthesis from T- helper 1 (Th1) cells. (269 aa)*
ATR	*Serine/threonine-protein kinase ATR; Serine/threonine protein kinase which activates checkpoint signaling upon genotoxic stresses such as ionizing radiation (IR), ultraviolet light (UV), or DNA replication stalling, thereby acting as a DNA damage sensor. Recognizes the substrate consensus sequence [ST]- Q. Phosphorylates BRCA1, CHEK1, MCM2, RAD17, RPA2, SMC1 and p53/TP53, which collectively*

	inhibit DNA replication and mitosis and promote DNA repair, recombination and apoptosis. Phosphorylates 'Ser-139' of histone variant H2AX at sites of DNA damage, thereby regulating DNA damage respon [...] (2644 aa)
FTH1	*Ferritin heavy chain, N-terminally processed; Stores iron in a soluble, non-toxic, readily available form. Important for iron homeostasis. Has ferroxidase activity. Iron is taken up in the ferrous form and deposited as ferric hydroxides after oxidation. Also plays a role in delivery of iron to cells. Mediates iron uptake in capsule cells of the developing kidney (By similarity). Belongs to the ferritin family. (183 aa)*
PRDX1	*Peroxiredoxin-1; Thiol-specific peroxidase that catalyzes the reduction of hydrogen peroxide and organic hydroperoxides to water and alcohols, respectively. Plays a role in cell protection against oxidative stress by detoxifying peroxides and as sensor of hydrogen peroxide-mediated signaling events. Might participate in the signaling cascades of growth factors and tumor necrosis factor-alpha by regulating the intracellular concentrations of H(2)O(2). Reduces an intramolecular disulfide bond in GDPD5 that gates the ability to GDPD5 to drive postmitotic motor neuron differentiation (By s [...] (199 aa)*
DDB2	*DNA damage-binding protein 2; Required for DNA repair. Binds to DDB1 to form the UV-damaged DNA-binding protein complex (the UV-DDB complex). The UV-DDB complex may recognize UV-induced DNA damage and recruit proteins of the nucleotide excision repair pathway (the NER pathway) to initiate DNA repair. The UV-DDB complex preferentially binds to cyclobutane pyrimidine dimers (CPD), 6-4 photoproducts (6-4 PP), apurinic sites and short mismatches. Also appears to function as the substrate recognition module for the DCX (DDB1-CUL4-X-box) E3 ubiquitin-protein ligase complex DDB1-CUL4-ROC1 (al [...] (427 aa)*
GSTP1	*Glutathione S-transferase P; Conjugation of reduced glutathione to a wide number of exogenous and endogenous hydrophobic electrophiles. Regulates negatively CDK5 activity via p25/p35 translocation to prevent neurodegeneration. (210 aa)*

Organism: Homo sapiens, NCBI taxonomy Id: 9606

Network

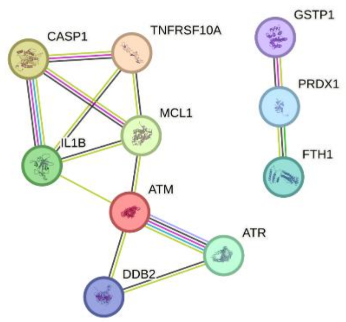

Network Stats

- number of nodes:10
- number of edges: 13
- average node degree: 2.6
- avg. local clustering coefficient: 0.767
- expected number of edges: 4
- PPI enrichment p-value: 0.000334

Biologic process (Gene Ontology)

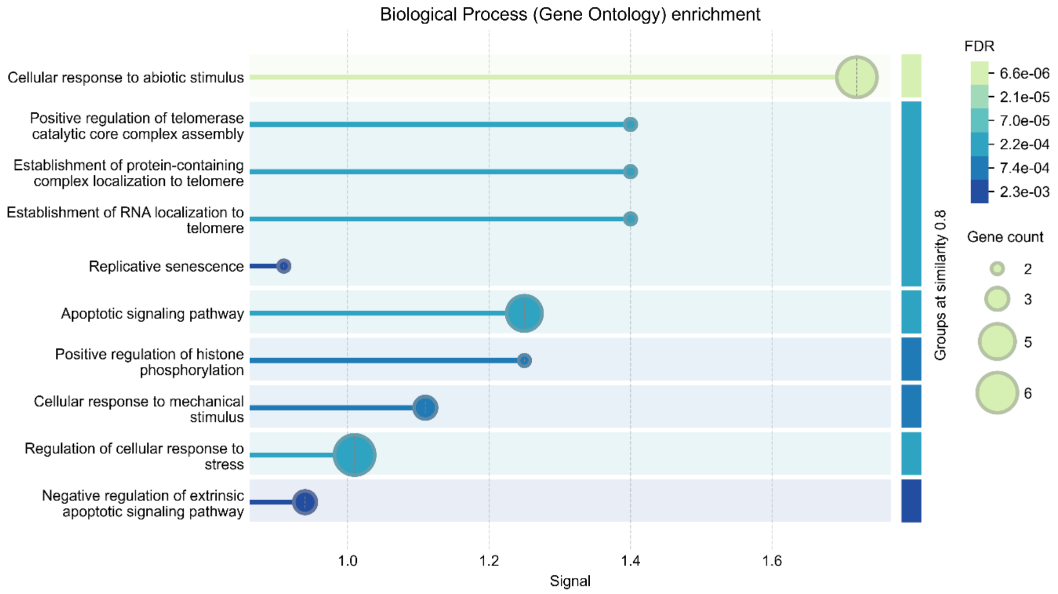

GO-term
description
count in network
strength
signal
false discovery rate
GO:0071214
Cellular response to abiotic stimulus
6 of 325
1.56
1.72
6.67e-05
GO:1904884
Positive regulation of telomerase catalytic core complex assembly
2 of 2
3.29
1.4
0.0036
GO:0097695
Establishment of protein-containing complex localization to telomere
2 of 2
3.29
1.4
0.0036
GO:0097694
Establishment of RNA localization to telomere
2 of 2
3.29
1.4
0.0036
GO:0097190
Apoptotic signaling pathway
5 of 318
1.49
1.25
0.0014
Reference Publications (PubMed)
publication

(year) title
count in network
strength
signal
false discovery rate
PMID:35741016
(2022) Lethal and Non-Lethal Functions of Caspases in the DNA Damage Response.
6 of 81
2.16
2.66
6.42e-06
PMID:34371724
(2021) Insight into the Web of Stress Responses Triggered at Gene Expression Level by Porphyrin-PDT in HT29 Human Colon Carcinoma Cells.
5 of 43
2.36
2.36
4.31e-05
PMID:28869497
(2017) Die Another Day: Inhibition of Cell Death Pathways by Cytomegalovirus.
5 of 47
2.32
2.34
4.36e-05
PMID:38217019
(2024) Role of reactive oxygen species in ultraviolet-induced photodamage of the skin.
5 of 58
2.23
2.16
8.82e-05
PMID:34888638
(2022) Parvovirus B19 induces cellular senescence in human dermal fibroblasts: putative role in systemic sclerosis-associated fibrosis.
4 of 17
2.67
2.16
0.00014

KEGG Pathways

pathway
description
count in network
strength
signal
false discovery rate
hsa04115
p53 signaling pathway
4 of 72
2.04
2.42
1.42e-05
hsa04217
Necroptosis
4 of 147
1.73
1.82
0.00011
hsa04210

Apoptosis
3 of 131
1.65
1.17
0.0040
hsa05164
Influenza A
3 of 163
1.56
1.06
0.0057
hsa05130
Pathogenic Escherichia coli infection
3 of 187
1.5
1.01
0.0068
Reactome Pathways
pathway
description
count in network
strength
signal
false discovery rate
HSA-3700989
Transcriptional Regulation by TP53
6 of 361
1.52
1.82
1.80e-05
HSA-5633008
TP53 Regulates Transcription of Cell Death Genes
3 of 43
2.14
1.5
0.0016
HSA-5218859
Regulated Necrosis
3 of 58
2.01
1.38
0.0025
HSA-6796648
TP53 Regulates Transcription of DNA Repair Genes
3 of 62
1.98
1.37
0.0025
HSA-448706
Interleukin-1 processing
2 of 9
2.64
1.31
0.0048
WikiPathways
pathway
description

count in network
strength
signal
false discovery rate
WP5119
NIPBL role in DNA damage - Cornelia de Lange syndrome
2 of 8
2.69
1.34
0.0043
WP4876
Activation of NLRP3 inflammasome by SARS-CoV-2
2 of 7
2.75
1.34
0.0043
WP3890
Nanomaterial-induced inflammasome activation
2 of 7
2.75
1.34
0.0043
WP3657
Hematopoietic stem cell gene regulation by GABP alpha/beta complex
2 of 20
2.29
1.31
0.0043
WP4925
Unfolded protein response
2 of 24
2.22
1.3
0.0043
Disease-gene Associations (DISEASES)
disease
description
count in network
strength
signal
false discovery rate
DOID:0050854
Muckle-Wells syndrome
2 of 4
2.99
1.03
0.0160
DOID:2987
Familial Mediterranean fever
2 of 7
2.75
1.02
0.0160
DOID:0090029
CINCA Syndrome
2 of 6
2.82

1.02
0.0160
Tissue Expression
tissue
description
count in network
strength
signal
false discovery rate
BTO:0000804
J-774A.1 cell
2 of 2
3.29
1.76
0.00084
BTO:0000583
Bone marrow cancer cell
6 of 442
1.43
1.64
3.15e-05
BTO:0001370
THP-1 cell
2 of 6
2.82
1.57
0.0017
BTO:0004732
Bone marrow-derived macrophage
2 of 8
2.69
1.47
0.0025
BTO:0000426
Erythroleukemia cell
4 of 244
1.51
1.23
0.0017
Protein Domains (Pfam)
domain
description
count in network
strength
signal
false discovery rate
PF02259
FAT domain
2 of 5
2.9
1.11
0.0112
Protein Domains and Features (InterPro)
domain
description
count in network
strength

signal
false discovery rate
IPR014009
PIK-related kinase
2 of 6
2.82
0.83
0.0349
IPR003152
FATC domain
2 of 6
2.82
0.83
0.0349
IPR003151
PIK-related kinase, FAT
2 of 5
2.9
0.83
0.0349
Protein Domains (SMART)
domain
description
count in network
strength
signal
false discovery rate
SM01343
The FATC domain is named after FRAP, ATM, TRRAP C-terminal (PMID:10782091). The solution structure of the FATC domain suggests it plays a role in redox-dependent structural and cellular stability (PMID:15772072).
2 of 6
2.82
1.29
0.0053

3. MONOCYTES

Input: IL1B

Organism: Homo sapiens, *NCBI taxonomy Id: 9606*

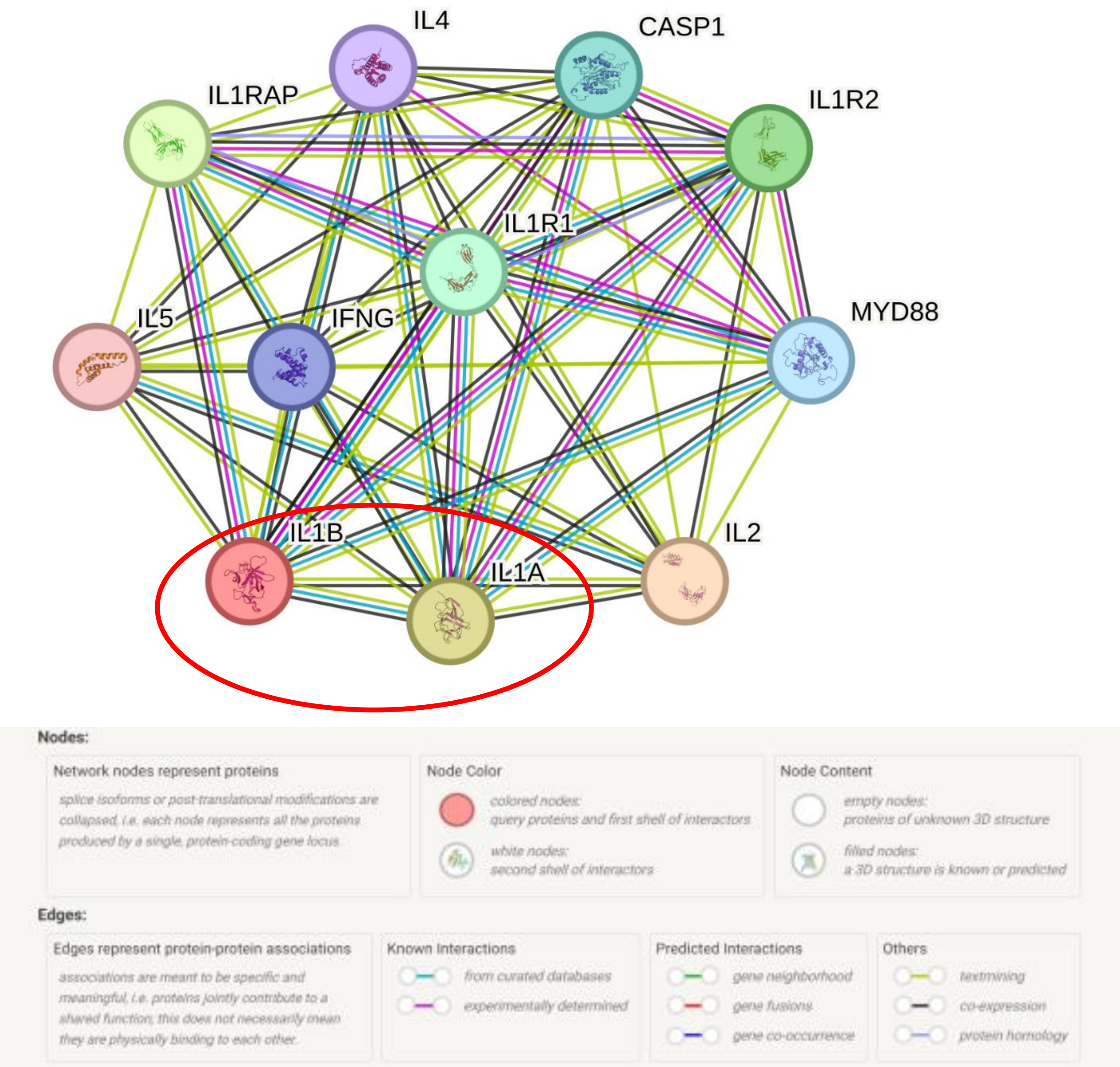

Network Stats

- Number of nodes: 11
- Number of edges: 53
- Average node degree: 9.64
- Avg. local clustering coefficient: 0.962
- Expected number of edges: 19
- PPI enrichment p-value: 7.02e-11

Biologic process (Gene Ontology)

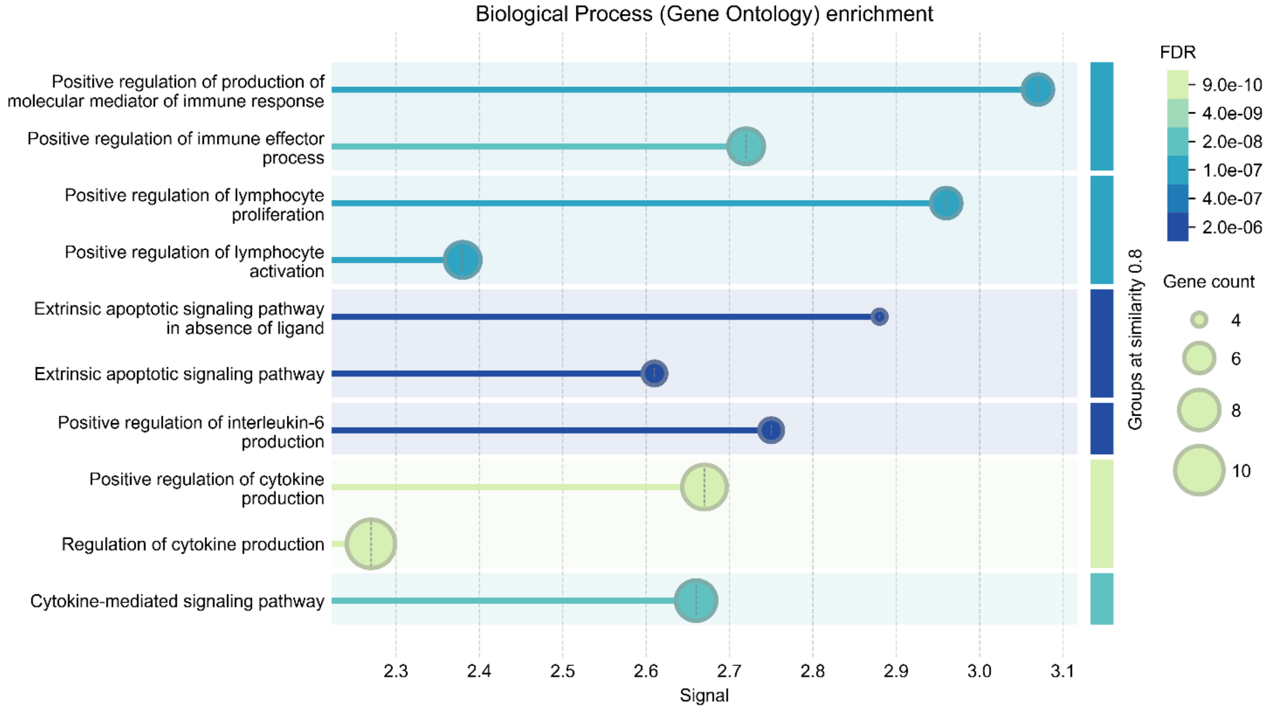

GO-term description

count in network
strength
signal
false discovery rate

GO:0002702
Positive regulation of production of molecular mediator of immune response
6 of 135
1.9
3.07
7.93e-08

GO:0050671
Positive regulation of lymphocyte proliferation
6 of 147
1.86
2.96
1.07e-07

GO:0097192
Extrinsic apoptotic signaling pathway in absence of ligand
4 of 36
2.3
2.88
2.26e-06

GO:0032755
Positive regulation of interleukin-6 production
5 of 98
1.96
2.75
1.04e-06

GO:0002699
Positive regulation of immune effector process
7 of 264
1.68
2.72
4.72e-08

Molecular Function (Gene Ontology)

GO-term
description
count in network
strength
signal
false discovery rate

GO:0070851
Growth factor receptor binding
8 of 135
2.03
4.67
5.03e-12

GO:0005149
interleukin-1 receptor binding
4 of 17
2.62
3.35
5.14e-07

GO:0005126
Cytokine receptor binding
8 of 270
1.72
3.29
5.56e-10

GO:0004908
interleukin-1 receptor activity
3 of 7
2.89
2.68
1.27e-05

GO:0005125
Cytokine activity
6 of 234
1.66
2.28
1.66e-06

Cellular Component (Gene Ontology)

GO-term
description
count in network
strength
signal
false discovery rate

GO:0005576
Extracellular region
10 of 4175
0.63
0.48
0.0034

Local Network Cluster (STRING)

cluster
description
count in network
strength
signal
false discovery rate

CL:15940
JAK-STAT signaling pathway, and Interleukin-1 family
9 of 138
2.07
5.57
1.38e-14

CL:16153
interleukin-1 receptor activity, and Interleukin-1 family
5 of 13
2.84
5.13
2.43e-10

CL:16155
Interleukin-1 conserved site, and Interleukin-1 receptor type 1
4 of 5
3.16
4.5
6.04e-09

CL:15945
JAK-STAT signaling pathway
4 of 63
2.06
2.26
2.58e-05

CL:15946
Interleukin-2 family signaling, and Interleukins 4 and 13
3 of 34
2.2
1.77
0.00041

KEGG Pathways

pathway
description
count in network
strength
signal
false discovery rate

hsa05321
Inflammatory bowel disease
6 of 59
2.26
4.72
1.06e-10

hsa04640
Hematopoietic cell lineage
6 of 90
2.08
4.11
5.78e-10

hsa05140

Leishmaniasis
5 of 69
2.11
3.56
2.48e-08
hsa04060
Cytokine-cytokine receptor interaction
8 of 282
1.71
3.39
1.06e-10
hsa05330
Allograft rejection
4 of 34
2.32
3.37
2.15e-07

Reactome Pathways

pathway
description
count in network
strength
signal
false discovery rate
HSA-446652
Interleukin-1 family signaling
8 of 149
1.98
4.69
1.67e-12
HSA-449147
Signaling by Interleukins
11 of 453
1.64
3.88
2.50e-15
HSA-9020702
Interleukin-1 signaling
6 of 111
1.99
3.55
7.91e-09
HSA-448706
Interleukin-1 processing
3 of 9
2.78
2.73
9.25e-06
HSA-6783783
Interleukin-10 signaling
4 of 45
2.2
2.7
4.18e-06

Disease-gene Associations (DISEASES)

disease
description

count in network
strength
signal
false discovery rate

DOID:0060496
Respiratory allergy
5 of 25
2.55
4.41
3.03e-09

DOID:1205
Allergic disease
6 of 72
2.17
4.06
2.20e-09

DOID:4483
Rhinitis
4 of 14
2.71
3.73
1.05e-07

DOID:974
Upper respiratory tract disease
5 of 67
2.13
3.27
1.47e-07

DOID:0060032
Autoimmune disease of musculoskeletal system
7 of 200
1.8
3.26

Tissue Expression

tissue
description
count in network
strength
signal
false discovery rate

BTO:0000155
Bronchoalveolar lavage fluid
4 of 7
3.01
4.18
2.10e-08

BTO:0003861
Inflammatory cell
4 of 14
2.71
3.75
9.70e-08

BTO:0000801
Macrophage
6 of 89
2.08
3.64

1.17e-08
BTO:0000878
Mononuclear cell
6 of 130
1.92
3.21
3.51e-08
BTO:0002417
Helper T-lymphocyte
4 of 28
2.41
3.13
9.09e-07

Subcellular Localization (COMPARTMENTS)

compartment
description
count in network
strength
signal
false discovery rate

GOCC:0043514
interleukin-12 complex
6 of 24
2.65
5.74
7.72e-12
GOCC:0045323
interleukin-1 receptor complex
4 of 7
3.01
4.35
9.95e-09
GOCC:0071735
IgG immunoglobulin complex
4 of 14
2.71
3.81
7.36e-08
GOCC:0070743
interleukin-23 complex
4 of 15
2.68
3.78
7.77e-08
GOCC:0099126
Transforming growth factor beta complex
4 of 20
2.55
3.57
1.60e-07

Annotated Keywords (UniProt)

keyword	description	count in network	strength	signal	false discovery rate
KW-0202	Cytokine	6 of 187	1.76	2.68	2.43e-07
KW-0395	Inflammatory response	5 of 163	1.74	2.21	6.31e-06
KW-0666	Pyrogen	2 of 2	3.25	1.96	0.00029
KW-0339	Growth factor	3 of 129	1.62	1.05	0.0063
KW-0964	Secreted	9 of 1839	0.94	0.99	6.31e-06

Protein Domains (Pfam)

domain	description	count in network	strength	signal	false discovery rate
PF02394	Interleukin-1 propeptide	2 of 2	3.25	1.34	0.0039

Protein Domains and Features (InterPro)

domain	description	count in network	strength	signal	false discovery rate

IPR004074
Interleukin-1 receptor type I/II
3 of 7
2.89
2.17
0.00011
IPR015621
Interleukin-1 receptor family
3 of 11
2.69
2.15
0.00011
IPR009079
Four-helical cytokine-like, core
4 of 56
2.11
2.01
0.00011
IPR035897
Toll/interleukin-1 receptor homology (TIR) domain superfamily
3 of 28
2.28
1.61
0.00093
IPR000157
Toll/interleukin-1 receptor homology (TIR) domain
3 of 27
2.3
1.61
0.00093

Protein Domains (SMART)

domain
description
count in network
strength
signal
false discovery rate
SM00255
Toll - interleukin 1 - resistance
3 of 17
2.5
2.1
0.00012
SM00125
Interleukin-1 homologues
2 of 10
2.55
1.16
0.0076